AGU PUBLICATIONS

Paleoceanography

RESEARCH ARTICLE
10.1002/2014PA002714

Key Points:
- ETNP records over 240 ka give new insight of the tropics' role in climate change
- Climate cycles of 2–6 ka prevail over the 1–2 ka/cycle over the last two glacials
- The pacing of millennial climate is amplified by oceanic and atmospheric processes

Supporting Information:
- Figures S1–S5 and Tables S1 and S2
- Data Set S1

Correspondence to:
E. Arellano-Torres,
elsa_arellano@ciencias.unam.mx

Citation:
Arellano-Torres, E., R. S. Ganeshram, L. E. Pichevin, and D. A. Salas-de-Leon (2015), Persistent millennial-scale climate variability in the eastern tropical North Pacific over the last two glacial cycles, *Paleoceanography*, *30*, 682–701, doi:10.1002/2014PA002714.

Received 22 AUG 2014
Accepted 15 MAY 2015
Accepted article online 19 MAY 2015
Published online 11 JUN 2015

Persistent millennial-scale climate variability in the eastern tropical North Pacific over the last two glacial cycles

Elsa Arellano-Torres[1,2], Raja S. Ganeshram[1], Laetitia E. Pichevin[1], and David Alberto Salas-de-Leon[3]

[1]School of Geosciences, University of Edinburgh, Grant Institute, Edinburgh, UK, [2]Now at Facultad de Ciencias, Universidad Nacional Autónoma de México, Mexico City, Mexico, [3]Instituto de Ciencias del Mar y Limnología, Universidad Nacional Autónoma de México, Mexico City, Mexico

Abstract High-resolution sediment records from the eastern tropical North Pacific (ETNP) spanning the last ~240 ka B.P. were studied to document the nature of millennial-scale climatic events in the tropical Pacific and to investigate teleconnection mechanisms. We present organic carbon (%OC) and diffuse spectral reflectivity records as indicative of upwelling and productivity changes off NW Mexico over the middle to late Pleistocene. The new productivity records document the persistence of abrupt millennial-scale changes over the last two glacial cycles. Detailed spectral and wavelet time series analyses show the predominance of longer climatic cycles (2–6 ka) during the last and the penultimate glacial periods. The persistence of millennial variability during the penultimate glacial, in absence of large ice rafted debris events in the North Atlantic, suggests that freshwater input through ice sheet dynamics is not essential for millennial-scale climate variability. Given the worldwide emerging picture of remarkable similar millennial-scale records over long time periods, we suggest that the pacing of this climate variability may represent a natural resonance in the climate system, amplified by a tightly coupled oceanic and atmospheric teleconnection processes. We present a schematic scenario of millennial-scale climate change depicting the role of the tropical Pacific in this global teleconnection system by linking productivity and upwelling changes in the ETNP with shifts in the position of the Intertropical Convergence Zone and the strength of the subtropical North Pacific High.

1. Introduction

Millennial-scale variations recorded in Greenland ice cores [*Dansgaard et al.*, 1993] and North Atlantic sedimentary records [*Bond et al.*, 1993] have shown abrupt transitions, from cold stadial states to warm interstadial states (i.e., Dansgaard/Oeschger or D/O events) during the last glacial period (~10–70 ka B.P.; i.e., marine isotope stages (MIS) 2–4). The sharp temperature increase between cold and warm phases in ice core records was about 10°C, occurring within a few decades [*Bond et al.*, 1993; *Dansgaard et al.*, 1984]. The disruption of the Atlantic Meridional Overturning Circulation (AMOC) caused by freshwater inputs through ice sheet calving, as marked by ice rafted debris (IRD) layers, was first assumed to be responsible for the abrupt temperature variations over the North Atlantic [*McManus et al.*, 1999]. Thus, freshwater inputs from such large ice armadas are associated with abrupt cooling in the North Atlantic (Heinrich events) [*Heinrich*, 1988; *MacAyeal*, 1993]. In addition, comparison of ice core temperature records from Greenland and Antarctica during the last glacial period revealed that cold events in the Northern Hemisphere (NH) were matched by progressive warming in Antarctica [*Blunier et al.*, 1998]. Such interhemispheric antiphasing is explained by the bipolar seesaw mechanism where disruption in the North Atlantic AMOC and the buildup of heat in the surface ocean leads to warming in southern latitudes [*Crowley*, 1992; *MacAyeal*, 1993]. These highlighted the global footprint of these abrupt climate swings revealing the susceptibility of the Earth to undergo large and abrupt climate changes relevant to human scale [*Blunier et al.*, 1998].

Although first reported in North Atlantic high-latitude records over the last glacial period, concomitant millennial-scale variations in the Earth's climate system were unearthed in midlatitude and low-latitude archives as well [*Behl and Kennett*, 1996; *Ivanochko et al.*, 2005]. In the NE Pacific, millennial-scale variations were first reported as changes in intermediate water oxygenation in laminated Santa Barbara Basin sediment sequences [*Kennett and Ingram*, 1995]. These sediments showed 17 distinct laminated intervals

that occurred frequently between 60 and 12 ka B.P. [*Behl and Kennett*, 1996], which were subsequently identified using benthic foraminifera assemblages as representing near anoxic conditions [*Cannariato et al.*, 1999] corresponding with warmer interstadial periods recorded in Greenland ice cores while bioturbated sequences deposited during stadial periods [*Dansgaard et al.*, 1984]. Subsequent studies in the NE Pacific (e.g., off Oregon, Santa Monica and Santa Barbara, the Baja California Peninsula, and the Gulf of California) identified millennial-scale variations. They are recorded in oxygen isotopes of planktonic foraminifera [*Hendy and Kennett*, 1999; *Hendy et al.*, 2004], sediment chemical composition [*Hendy et al.*, 2004; *Hendy and Pedersen*, 2005], and nitrogen isotopes [*Emmer and Thunell*, 2000; *Hendy and Pedersen*, 2005] recording a range of environmental changes including the strength of the oxygen minimum zone [*Cannariato et al.*, 1999], sea surface temperatures and thermocline depths [*Hendy and Kennett*, 1999], intermediate water masses [*Stott et al.*, 2000], sediment redox conditions [*Hendy and Pedersen*, 2005; *van Geen et al.*, 2003], subsurface denitrification [*Emmer and Thunell*, 2000], upwelling strength, and marine productivity [*Ortiz et al.*, 2004].

Millennial-scale variations are now thought to be pervasive in the tropical hydrological cycle [*Overpeck and Cole*, 2006], as changes in monsoon intensity and/or in the latitudinal position of Intertropical Convergence Zone (ITCZ) in the Atlantic, Pacific, and Indian Oceans [*Hendy and Kennett*, 1999; *Hendy et al.*, 2002; *Ivanochko et al.*, 2005; *Ortiz et al.*, 2004; *Peterson et al.*, 2000]. These studies have drawn a link between temperature changes in Greenland and the North Atlantic with the latitudinal migration of the ITCZ in the tropics [e.g., *Bond et al.*, 1993; *Dansgaard et al.*, 1993; *Keigwin and Jones*, 1994]. The Earth's hydrological cycle perturbations are suggested to have caused large-scale redistribution of heat and moisture on the surface with global consequences. Another diagnostic feature of the millennial-scale climate variability is the abrupt variations in atmospheric greenhouse gas (GHG) concentrations (i.e., water vapor, carbon dioxide, methane, and nitrous oxide) recorded in ice cores [*Intergovernmental Panel on Climate Change*, 2007]. For instance, interstadial increases of CH_4 production, thought to derive mainly from low-latitude wetlands, occurred in tandem with the northern migration of ITCZ and enhanced monsoon intensity recorded in marine and terrestrial records [*Flückiger et al.*, 1999; *Flückiger et al.*, 2004; *Ivanochko et al.*, 2005]. These abrupt shifts in the position of the ITCZ and GHG emission point to the tropics as an amplifier of the millennial-scale climate changes, if not the trigger. However, teleconnection mechanisms (atmospheric and/or oceanic) between low and high latitudes at millennial scales are still unclear [*Chiang*, 2009].

Because abrupt climate changes were first observed in the NH high latitudes and the North Atlantic, variations in the strength of the AMOC were first assumed to be responsible for the large variations in temperature over the North Atlantic [*Bond et al.*, 1993]. However, with the discovery that the tropics have undergoing similar variations, and given the size of the tropical ocean compared to the North Atlantic and its ability to trigger global climatic perturbations today [*Cane*, 1998; *Clement et al.*, 1999; *Siddall et al.*, 2006], it was subsequently proposed that abrupt climate changes were originated and propagated from low latitudes via a range of atmospheric and oceanic processes [*Clement et al.*, 1999; *Haug et al.*, 2001; *Koutavas et al.*, 2002; *Leduc et al.*, 2009; *Stott et al.*, 2002]. For instance, perturbations such as El Niño–Southern Oscillation (ENSO) originate in the equatorial Pacific and have global climatic repercussions. However, recent modeling studies reveal that abrupt AMOC slowdown has climatic impacts that can extend globally. Such models show that the resultant cooling in the NH causes an interhemispheric thermal gradient which in turn gives rise to a southward shift of the ITCZ in the Atlantic [*Stouffer et al.*, 2006; *Vellinga and Wood*, 2002].

Most of the NH records with sedimentation rates high enough to resolve millennial-scale events do not extend beyond the penultimate interglacial period (~123 ka B.P.; i.e., MIS 5), besides it also marks the termination of the Greenland ice cores [*Broecker*, 1992; *Curry and Oppo*, 1997]. On the other hand, millennial-scale sea surface temperature (SST) records extending beyond MIS 7 have been reconstructed in marine sediments from the Iberian Margin, in North Atlantic midlatitudes [*Martrat et al.*, 2007], but equivalent records from the tropical Pacific Ocean are scarce despite its recognized sensitivity to record global climatic perturbations [*Cane*, 1998; *Clement et al.*, 1999]. This represents a major gap in our knowledge for understanding the nature of these abrupt climate variations. In this study, we present new, high-resolution sediment core records from the eastern Tropical North Pacific (ETNP) spanning the last two climatic cycles (i) to document and understand the nature of the millennial-scale climatic events in the

tropical Pacific, and (ii) to investigate the relationship between low- and high-latitude records beyond the last climatic cycle extending to ~240 ka B.P., covering the penultimate glaciation (marine isotope stage 6).

1.1. Study Area

Today, along the NE Pacific margins off California and NW Mexico, the climate is influenced by the location and seasonal migration of the ITCZ, subtropical North Pacific High, and the Aleutian Low [*Bakun and Nelson*, 1991; *Barry and Chorley*, 2003]. The study area is in boundary of the California Current System to the north, which is a typical eastern boundary current system with equatorward surface flow of cold California Current (CC) and subsurface (100–300 m) poleward flow of California Undercurrent, and the tropical waters of the Costa Rica Coastal Current (CRCC) to the south. In winter, the study area is under the influence of the CC. During boreal summer and fall, the CC moves north by 10° controlled by the migration of the ITCZ, bringing the study area under the influence of the Costa Rica Coastal Current (CRCC) which expands to the tip of the Baja California Peninsula [*Badan-Dangon*, 1998; *Kessler*, 2006].

Locally, the southward shore-parallel winds caused by air pressure differences between the North Pacific High pressure system (subtropical High, hereinafter), and the thermal Low centered on the continent drive coastal upwelling in winter and early spring off NW Mexico [*Badan-Dangon*, 1998; *Kessler*, 2006; *Lavin et al.*, 1995; *Reyes and Lavin*, 1997; *Wyrtki*, 1965]. Past changes in coastal upwelling off NW Mexico is thought to be sensitive to myriad of factors including meridional temperature gradients, the north-south migration of the ITCZ, ENSO oscillations, the mean position and the intensity of the subtropical High, the relative position of the jet stream, and the presence of Laurentide ice sheet on land [*Cheshire et al.*, 2005; *Ganeshram and Pedersen*, 1998; *Hendy and Kennett,* 1999, 2003; *Kutzbach et al.*, 1998; *McClymont et al.*, 2012] In the modern, shore-parallel winds and upwelling off Southern California and NW Mexico occur when ITCZ and the subtropical High are in the southern position in winter and early spring; but they wane in summer, when ITCZ shifts north and the subtropical High intensifies and expands to temperate latitudes. This seasonal pattern is profoundly altered during glacial periods. Climate model simulation shows that the presence of the Laurentide ice sheet and the semipermanent glacial anticyclonic High over the ice sheet had a profound influence of the wind patterns during glacial periods [*Ganeshram and Pedersen*, 1998; *McClymont et al.*, 2012].

In the ETNP (NW Mexico), coastal upwelling fuels high biological productivity and high carbon exports through the water column and sediments. Consequently, the sediments are organic rich and often laminated typifying upwelling sedimentary facies [*Ganeshram et al.*, 1999]. The Oxygen Minimum Zone off NW Mexico is particularly intense with near-zero oxygen levels extending between 200 and 800 m water depth supporting water column denitrification [*Brandes et al.*, 1998; *Ganeshram et al.*, 2000], thus suggesting that surface productivity, driven by the local upwelling, exerts an important control on the oxygenation of the water column [*Ganeshram et al.*, 1995, 2000].

2. Material and Methods

The piston cores MD02-2518 (latitude 22°40.39′N; longitude 106°29.19′W; 450 m water depth) and MD02-2519 (latitude 22°30.89′N; longitude 106°39.00′W; 955 m water depth) were retrieved from the continental slope off Mazatlan, Mexico (Figure 1), during the IMAGES IV (*International Marine Global Past Change Studies*) MONA (Marges Ouest Nord-Américaines) oceanographic expedition [*Beaufort*, 2002]. The total length of cores MD02-2518 and MD02-2519 is 4000 and 3600 cm, respectively. The sediment sequences consist of massive to laminated intervals, and none of the cores show disturbance or hiatuses in the stratigraphic description. The laminations range from fine (0.5–2 mm) to thicker banding (5–20 mm) that sometimes alternate with faintly bioturbated intervals. The cores sites are located in the ETNP within an intense oxygen-minimum zone (OMZ) that extends from ~150 to 800 m depth with almost undetectable O_2 concentrations between 150 and 600 m water depth ($[O_2] < 10\ \mu M$) [*Ganeshram et al.*, 1999]. At the surface, the region experiences intense winter upwelling in response to the intensification shore-parallel winds, high levels of biological productivity, and elevated export production [*Bakun and Nelson*, 1991; *Roden*, 1962]. In turn, the sediment sequences reflect these conditions, being extremely rich in organic carbon (%OC > 7%) and other biogenic components [*Ganeshram and Pedersen*, 1998].

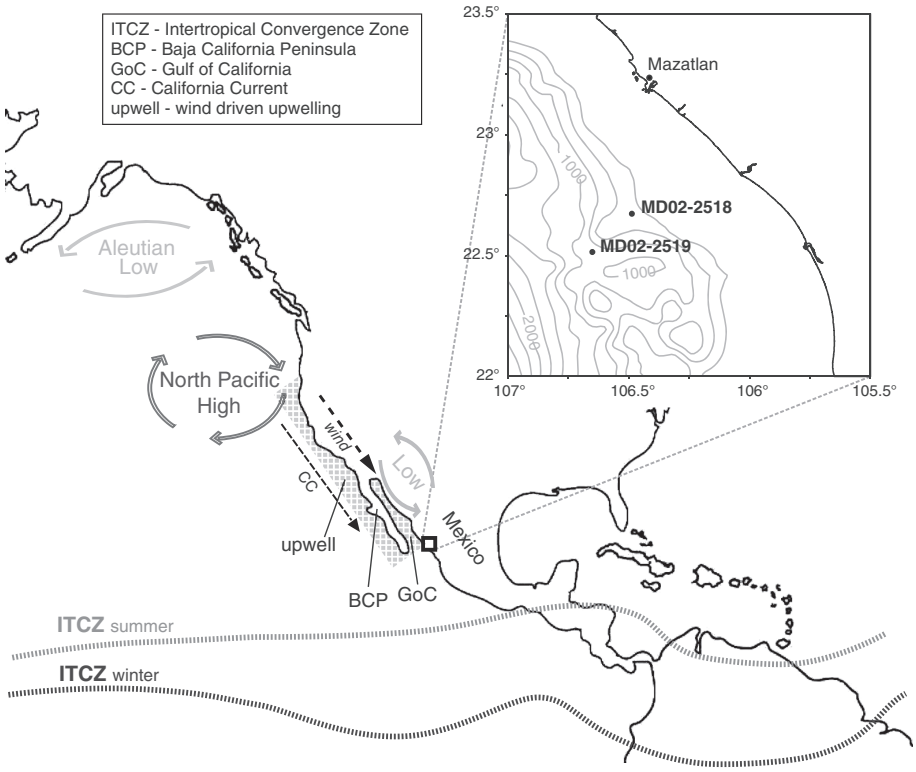

Figure 1. Map of the study area showing a generalized illustration of the modern large-scale atmospheric circulation, the coastal upwelling, and the ITCZ average position during summer and winter (www.opc.ncep.noaa.gov). Inset: location of the cores MD02-2518 (latitude 22°40.39′N; longitude 106°29.19′W; 450 m water depth) and MD02-2519 (latitude 22°30.89′N; longitude 106°39.00′W; 955 m water depth).

2.1. Paleoceanographic Proxies

Sample analyses of bulk organic carbon (OC) from marine sediments and oxygen isotopes of benthic foraminifera (δ^{18}O-BF) were performed in the Wolfson Laboratory at the School of Geosciences, the University of Edinburgh. To perform the carbon-nitrogen (C-N) analyses, the cores were subsampled at every 1–2 cm for the Core MD02-2518 and every 2 cm for the Core MD02-2519. The sediments were freeze dried, ground, and homogenized in an agate mortar. To remove all traces of carbonates, the samples were acidified with HCl (5%) on a hot plate at 70°C. The percentage of organic carbon (%OC) was analyzed using a Carlo Ebra NA2500 C-N elemental analyzer in line with a VG PRISM III isotope ratio mass spectrometer. An acetanilide standard was used for elemental compositions, where its values are carbon 71.09% and nitrogen 10.36%. The PRISM III elemental analysis software uses the K-Factor method to calculate sample elemental composition by comparison with the acetanilide standard. The elemental analysis error was ±1.3% for carbon.

Analyses of δ^{18}O in the Core MD02-2519 were performed in sediment samples chosen every 2–5 cm in the first half of the core (0–1800 cm) and every ~10–20 cm in the second half (1800–3600 cm), depending on the foraminifera abundances. All sediment samples were routinely washed with running water through a 65 μm mesh size to eliminate the finer fraction. About 10 shells of *Uvigerina* spp. were carefully picked, rinsed, and sonicated for few seconds in double-distilled water for isotopic analyses. The handpicked carbonate sample was reacted with 100% orthophosphoric acid at 75°C in a "Kiel Carbonate III" preparation device. The resulting CO_2 was analyzed on a *Thermo Electron Delta$^+$ Advantage* stable isotope ratio mass spectrometer. The laboratory standard marble powder (MAB2B) run as a sample between November 2006 and April 2008 was $\delta^{18}O_{PDB} = 19.40 \pm 0.07‰$. All isotopic values are quoted relative to standard Pee Dee belemnite.

The diffuse spectral reflectivity (DSR) was measured on board the ship at every 2 cm with a Minolta-2022 spectrophotometer [*Beaufort*, 2002]. The parameter *a** (the *red/green* attribute) was calculated

Table 1. Age Controls Used to Construct the Age Model of Cores MD02-2518 and MD02-2519[a]

Age Model: Core MD02-2518

Source	MD02-2518 Depth (cm)	Age (Cal ka B.P.)	Source (Symbol)
AMS ^{14}C	10	1.2	x
AMS ^{14}C	140	6.7	x
AMS ^{14}C	230	11.2	x
AMS ^{14}C	260	13.8	x
AMS ^{14}C	284	18.9	x
AMS ^{14}C	340	33.2	x
AMS ^{14}C	372	36.2	x
AMS ^{14}C	422	44.0	x
GISP2-D/O 12	490	45.3	◊
GISP2-D/O 14	590	51.9	◊
GISP2-D/O 17	664	57.5	◊
GISP2-D/O 19	954	68.4	◊
GISP2-D/O 21	1250	83.6	◊
GISP2-D/O 23	1534	101.0	◊
GISP2-D/O 25	1712	108.1	◊
ODP 977A-(MIS 5e) 26	1906	121.6	◊
ODP 977A-(MIS 6.0) S1′	1990	130.0	◊
ODP 977A-(MIS 6.4) S4′	2376	150.3	◊
ODP 977A-(MIS 6.6) 9′	2930	180.8	◊
ODP 977A-(MIS 7a) 11′	3146	193.4	◊
ODP 977A-(MIS 7c) 12′	3560	215.5	◊
ODP 977A-(MIS 7d) 13′	3836	224.5	◊

Age Model: Core MD02-2519

Source	MD02-2519 Depth (cm)	Age (Cal ka B.P.)	Source (Symbol)
AMS ^{14}C	1	2.4	+
AMS ^{14}C	74	3.8	+
AMS ^{14}C	140	6.3	+
AMS ^{14}C	194	9.1	+
AMS ^{14}C	216	10.2	+
AMS ^{14}C	230	11.1	+
AMS ^{14}C	284	13.9	+
AMS ^{14}C	290	14.1	+
AMS ^{14}C	332	16.1	+
AMS ^{14}C	370	18.5	+
AMS ^{14}C	424	21.4	+
AMS ^{14}C	466	23.2	+
AMS ^{14}C	500	25.7	+
AMS ^{14}C	558	28.2	+
AMS ^{14}C	576	28.8	+
AMS ^{14}C	606	30.5	+
AMS ^{14}C	636	32.5	+
AMS ^{14}C	676	34.5	+
AMS ^{14}C	758	39.5	+
GISP2-D/O 12	870	45.3	°
GISP2-D/O 14	956	51.9	°
GISP2-D/O 17	1044	57.5	°
GISP2-D/O 18	1138	61.9	°
GISP2-D/O 19	1272	68.4	°
GISP2-D/O 20	1316	72.8	°
GISP2-D/O 21	1428	83.6	°
GISP2-D/O 23	1630	101.1	°
GISP2-D/O 25	1744	108.1	°
ODP 977A-(MIS 6.0) S1′	2070	130.0	°
ODP 977A-(MIS 6.2) 1′	2156	137.0	°
ODP 977A-(MIS 6.4) S4′	2458	151.3	°
ODP 977A-(MIS 6.5) 8′	2824	175.1	°
ODP 977A-(MIS 6.6) 9′	3040	180.8	°

[a]AMS ^{14}C dates are detailed in the supporting information Table S1 (crosses and plus signs as in Figure 2). Identified D/O events correspond to the classification of GISP2 and ODP-977A (diamond and circle symbols as in Figure 2). D/O, Dansgaard/Oeschger, S, Stadial, and MIS, Marine.

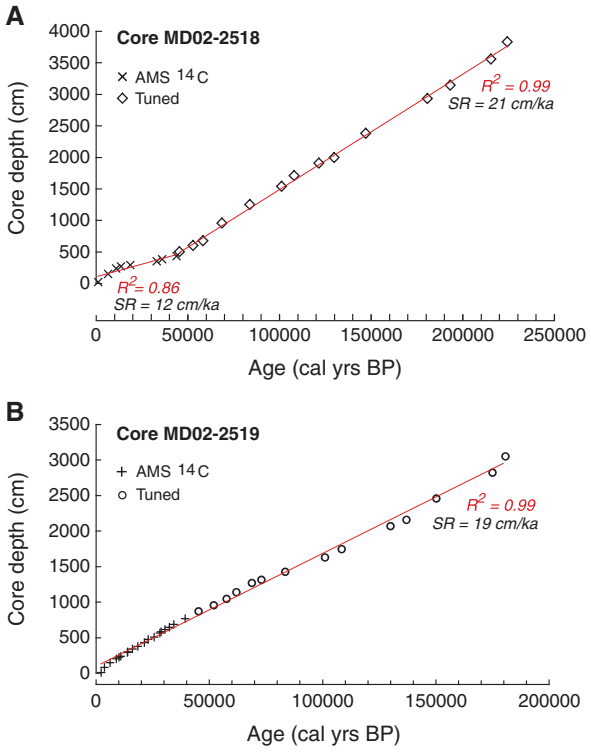

Figure 2. Age model of the sediment cores (a) MD02-2518 and (b) MD02-2519, including AMS ^{14}C and tuned ages. Symbols are age control points: crosses and plusses signs from radiocarbon dates; diamonds and circles from estimated dates based on the GISP2 and ODP-977A scales [*Grootes and Stuiver*, 1997; *Martrat et al.*, 2004]. Red line is the average sedimentation rate (SR) (see Table 1 for details).

automatically with the spectrophotometer. The DSR is a nondestructive technique used to obtain a rapid assessment of the geochemical composition [*Ortiz et al.*, 1999] and provides a semiquantitative assessment of the sediment components [*Mix et al.*, 1992]. The method has shown to be particularly useful in regions with organic-rich sediments in the NE Pacific margin, where different color attributes have been successfully linked to %OC and other present components (e.g., %$CaCO_3$ or terrigenous sediments) [*Ortiz et al.*, 1999, 2004]. Following these studies, we used the DSRa* as a semiquantitative indicator of %OC based on (1) the similarity between the DSRa* and the %OC records in the cores MD02-2518 and MD02-2519, over the last 120 ka B.P., (2) the high-correlation coefficients calculated between the %OC and the DSRa* (i.e., 0.76 in Core MD02-2518 and 0.60 in Core MD02-2519). On this basis, the DSRa* curve is used as a proxy of %OC in older intervals.

2.2. Age Model Construction and Sedimentation Rates

The age models constructed for the cores MD02-2518 and MD02-2519 (Table 1) denote regular sedimentation rates (SR) and linear age versus depth relationships (R^2 = 0.86 to 0.99) (Figure 2). For %OC analysis, the Core MD02-2518 was subsampled every 1–2 cm, thus showing average sampling resolutions of ~80–250 years/sample; whereas the Core MD02-2519 was subsampled every 2 cm, thus showing ~60–150 years/sample. Although an inflection point on the slope is identified at 50 ka B.P. in Figure 2a (i.e., Core MD02-2518), it cannot be explained as an artifact of the age model based on radiocarbon, but to a slight change in the sedimentation rate. This is demonstrated through the construction of an age model completely tuned to GISP2 (Greenland Ice Sheet Project 2) (see supporting information), which shows a similar inflection point at this time. Furthermore, the average SR between 12–20 cm/ka and ~19 cm/ka of the cores MD02-2518 and MD02-2519 (respectively) largely agree with previous studies in sediment records off NW Mexico [*Ganeshram and Pedersen*, 1998]. Based on the graphic correlations to Greenland and the North Atlantic, Core MD02-2519 extends back to MIS 6.6 and the Core MD02-2518 up to MIS 7d. Further, the δ^{18}O-*Uvigerina* record independently verified this (see supporting information).

2.3. Spectral and Wavelets Analyses

Spectral analyses were performed using the software *Analyseries 2.0.8* [*Paillard et al.*, 1996] to extract the major time frequencies present in the records. To further validate the results, they were independently extracted with *SPECTRUM 2.2* [*Schulz and Stattegger*, 1997]. The results obtained by using the two different software packages were similar. Comparisons were made on the results of spectral analyses between cores from low and high latitudes, between the last glacial period (MIS 2–4), the last interglacial period (MIS 5), and the penultimate glacial period MIS 6.

Time series analyses were applied to the DSRa* records of both cores. The orbital trend was removed (by applying a 7000 years running average, similar to *Barker et al.* [2011]) to show a much clearer correspondence of the millennial-scale events. The last two glacial periods (MIS 2–4 and 6) as well as the last interglacial (MIS 5) were independently analyzed to obtain specific periodicities. The first glacial

interval is centered between 15 and 70 ka B.P. (corresponding to MIS 2–4), and the second between 130 and 185 ka B.P. (corresponding to MIS 6). The interglacial interval MIS 5 spans 75–125 ka B.P. The spectral analyses performed with Analyseries followed two classical methods, Blackman Tukey (B Tukey) and Maximum Entropy (MEM). The "input" data set for each spectral analysis was "resampled" to obtain an even time resolution (every 100 years) by applying cubic spline simple interpolation. The linear trend of the series was removed and "default" prewhitening was applied. The B Tukey method (based on standard Fourier transform) was used to obtain the linear power spectrum and to identify the main linear oscillations (Tukey window function with bandwidth of 0.23 cycles/ka, explaining 50% of series). In addition, the MEM method was applied to increase the resolution of the spectral peaks (explaining 30% of series). To determine the statistical significance of the frequencies obtained (i.e., not noise signals), *F* tests were performed using a MTM (Multitaper Method). Only frequencies with >90% confidence level were accepted (i.e., *F* test > 0.90 in the output frequencies between 5×10^{-5}–1×10^{-3} cycles/ka) and compared with the SPECTRUM results.

The harmonic analyses performed with SPECTRUM (analogous to that of autospectral analysis) did not require resampled input data as the software is designed for unevenly spaced time series (based on Lomb-Scargle Fourier transform and Welch overlapped segment averaging procedure [*Schulz and Stattegger*, 1997]). The default oversampling factor and the highest frequency were used in all analyses; they were tested for two to three harmonic components using a significance level of 0.05, the linear trend was removed. After we verified and selected the major spectral peaks of each time interval (15–70 ka, 75–125, and 130–185 ka), we cleaned the series with a band-pass Gaussian filter centered at the frequencies obtained with MEM. The combined sum of Gaussian filters (bandwidth = 0.2×10^{-4}) was used to identify the pacing and principal features of the series. The two time series analysis methods produced comparable results. Finally, the DSRa* records were examined with wavelet analysis to determine the nonstationary periodicities of the time series. Such a property is identified by the change in the slope of the spectral curve, as an indicative of phase variations in the low frequencies that represent groups of stationary and nonstationary waves. The Morlet method was applied to the wavelet analysis as it is commonly used to locate variations of power within the time series. The Morlet method consists of a plane wave modulated by a Gaussian function, which decomposes the series into time-frequency spaces to determine both, the dominant modes of variability (phase changes) and how those modes change in time. We applied this method using the default settings of the online software developed by *Torrence and Compo* [1998]. Only values inside the 90% cone of influence (COI) were considered significant.

3. Results

3.1. A 240 ka Reconstruction of Paleoproductivity Variations in the ETNP

We present two continuous records of paleoproductivity changes spanning the last ~240 ka B.P. based on high-resolution %OC measurements combined with DSRa* data (Figure 3). As previously shown in the Magdalena margin of Baja California (Mexico) by *Ortiz et al.* [2004], the color attribute of the sediments displays similarity to the %OC in these highly productive organic-rich sediment sequences. Therefore, this parameter represents a continuous, semiquantitative record of organic carbon content, which we used here to extend our reconstructions beyond MIS 5. At present, the ETNP experiences high levels of primary productivity when cold, nutrient-rich water is brought to the surface by Ekman transport. Here the upwelling is predominantly wind driven, thus coupled to prevailing atmospheric patterns and hence sensitive to climate change [*Hendy et al.*, 2004; *Ortiz et al.*, 2004]. In upwelling-dominated settings such as the ETNP, high levels of organic matter are exported from the surface in the form of organic debris. This intensifies oxygen depletion in the water column (via organic carbon oxidation) and induces the development of reducing conditions in the sediments, as well as enhanced preservation of sedimentary organic carbon. Thus, organic matter production and sedimentary preservation are highly coupled to upwelling in the ETNP margin [*Ganeshram et al.*, 1999]. Previous studies off the coast of NW Mexico and California have shown that %OC behave similarly to other productivity proxies such as bio-barium, sedimentary trace elements, carbonate concentrations, planktonic foraminifera assemblages, and, therefore, can be considered a faithful marker of upwelling-induced paleoproductivity in our study area [*Ganeshram and Pedersen*, 1998; *Hendy et al.*, 2004; *Hendy and Pedersen*, 2005]. Hence, we interpret %OC (and DSRa*) in the cores collected off NW Mexico as proxies for productivity variations linked to upwelling intensity.

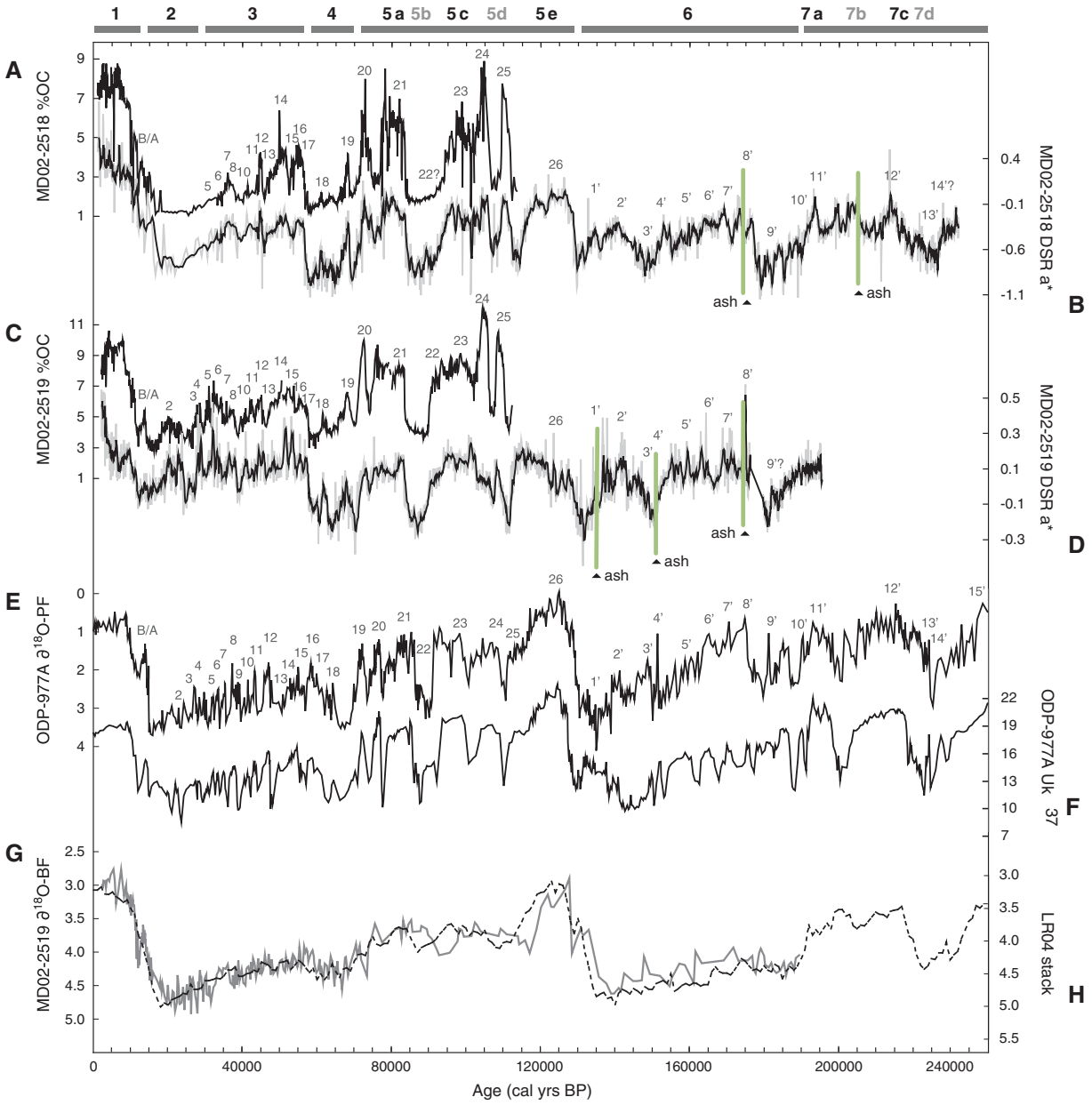

Figure 3. Records spanning the last two glacial cycles (0–240 ka). Band on top shows glacial-interglacial MIS 1–7d. (a) %OC and (b) DSRa* records of Core MD02-2518 (black line, five-point moving average). The ash layers are placed at 173.4 and 205.0 ka B.P. (c) %OC record and (d) DSRa* records of Core MD02-2519 (black line, five-point moving average). The ash layers are placed at 137.0, 152.3, and 175.1 ka B.P. (e) δ^{18}O-*Globigerina bulloides* and (f) sea surface temperature ($U^{K'}37$) records of Core ODP-977A [*Martrat et al.*, 2004]. (g) δ^{18}O-*Uvigerina* spp. record of Core MD02-2519 (solid line). (h) LR04 δ^{18}O stack record of Lisiecki and Raymo [2005] (broken line). Numbers between 0 and 130 ka are referred to D/O events (1–26). Numbers between 130 and 240 ka are interstadials (1′–15′), marked with a question mark (?) when doubtful.

The marine sediment cores MD02-2518 and MD02-2519 display frequent and large shifts in %OC and DSRa* (Figures 3 and 4). The OC varies between 1–8.9% and 2.7–12% in each core, respectively. Higher values of organic carbon are seen during interglacials and Greenland interstadials (i.e., warm periods), while 2–3 times lower values are seen during glacials and stadials, including Heinrich events (i.e., cold periods). Maximum values ($OC_{MD02\text{-}2518} > 6\%$; $OC_{MD02\text{-}2519} > 8\%$) in OC records are observed during MIS 5 and the Holocene. Both cores have the lowest values (<2–3%) over MIS 2, 4, and 5b. The patterns of OC-MAR variation are similar to the %OC record, given the linear sedimentation rates in Core MD02-2519 and most part of MD02-2518 (Figure 2); therefore, they are not shown.

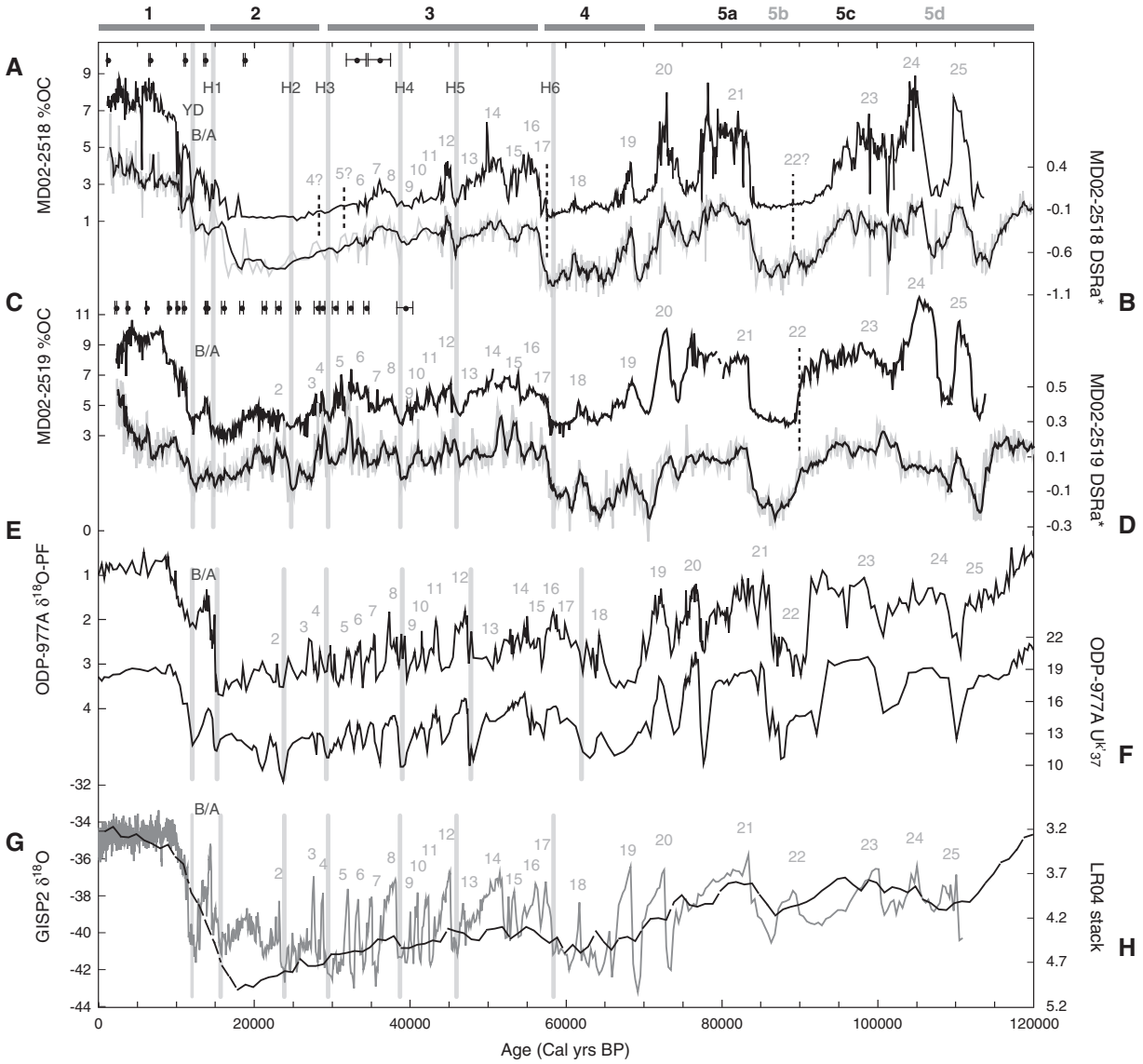

Figure 4. Comparison between records over the last glacial cycle (0–120 ka). Band on top shows MIS 1–5d. (a) %OC and (b) DSRa* records of Core MD02-2518 (black line, five-point moving average); (c) %OC and (d) DSRa* records of Core MD02-2519 (black line, five-point moving average); (e) δ^{18}O *Globigerina bulloides* and (f) SST $U^{k'}_{37}$ records of Core ODP-977A; (g) GISP2 δ^{18}O record; (h) LR04 δ^{18}O stack record. Dots with error bars are AMS ^{14}C dates. Numbers are D/O 1–25; vertical grey lines are the YD and Heinrich events H1–H6 [*Bond et al.*, 1999].

The OC and DSRa* records both show well-defined millennial-scale oscillations that can be easily matched with events identified in Greenland and North Atlantic temperatures. Therefore, the OC and DSRa* records are used to construct the age model of Core MD02-2519 and extend the chronology up to the penultimate glacial cycle (~240 ka B.P.). The millennial-scale events identified in the %OC and DSRa* records are numbered following the GISP2 and the Ocean Drilling Program (ODP)-977A terminology. The 26 events of the last climate cycle (0–130 ka B.P.) correspond to interstadial Dansgaard/Oeschger events (D/O 1–26) [*Dansgaard et al.*, 1993] (Figure 4). The 15 events beyond D/O 26 correspond to interstadial events (I-1′ to 15′) during the penultimate glacial period (~130–240 ka B.P.) [*Martrat et al.*, 2004]. In the course of MIS 2, MIS 4, and MIS 5b, some of the millennial-scale events are better resolved in the %OC record of Core MD02-2519 than in the Core MD02-2518 during D/O 2, 3, 4, 15, 17, 18, and 22, possibly aided by the higher-glacial sedimentation rate in this core. However, the resolution of the color reflectivity record of both cores is high enough to reveal all D/O events; thus, the DSRa* record enables us to extend the records age model up to I-9′ in Core MD02-2519 and up to I-25′ in Core MD02-2518.

Both the timing and intensity of the observed millennial-scale changes in %OC closely match the temperature variations recorded in the high latitudes, with high-productivity episodes occurring during interstadial events (Figures 3 and 4). As suggested by previous studies in the NE Pacific, such synchronicity between records reveals that an intimate relationship exists between NH distant regions via atmospheric and/or oceanic processes [*Hendy et al.*, 2002]. In the following sections, we further explore the synchronicity between the millennial-scale changes recorded in the low-latitude upwelling/productivity and the midlatitude to high-latitude temperature records, in order to tease out the teleconnection mechanisms in the ocean-atmosphere climate system over the last and the penultimate glacial cycles. For that purpose, we apply spectral and wavelets analyses to thoroughly compare the pacing of these abrupt events in low latitude, midlatitude, and high latitude during the last and the penultimate glacial (i.e., MIS 2–4 and MIS 6, respectively), and the penultimate interglacial (MIS 5). Finally, we compare our ETNP records with CH_4 and N_2O records from ice cores (i.e., GISP2 and Byrd-EPICA) to illustrate the relationship between these climate records.

In Figure 3, records from the ETNP cores are compared with alkenone (Uk'_{37})-based SST records from Core ODP-977A from the Iberian Margin (North Atlantic). During MIS 6 and 7, the millennial-scale variations in % OC seen in our records correspond to SST changes recorded in Core ODP-977A, very much similar to the last glacial period (Figure 3). On longer time scale, DSRa* show a gradual reduction in the red/green attributes down core due to organic decomposition (e.g., photosynthetic pigments) and/or compaction in Core MD02-2519. Although this represents a disadvantage for using the sediment color properties to quantify %OC down core, it does not obscure the existence of millennial-scale events during MIS 6 and MIS 7.

The first finding that can be drawn from our new records is that the ETNP experienced abrupt climatic, atmospheric, and/or hydrological reorganization during the penultimate glacial period at millennial-scale scales, similar to the last glacial cycle. This suggests that millennial-scale variations are persistent throughout MIS 6–MIS 7 similar to those documented over the midlatitude to high latitude as previously shown [*Altabet et al.*, 2002; *Martrat et al.*, 2004, 2007; *Oppo et al.*, 1998; *Pahnke and Zahn*, 2005]. Documentations of millennial-scale events in the low latitudes such as the ETNP beyond the last glacial period are rare, due to the scarcity of long and high-resolution records that usually do not extend beyond MIS 5 [*Bar-Matthews et al.*, 2003; *Cartapanis et al.*, 2014; *Yuan et al.*, 2004]. Therefore, our new records from the NW Mexican margin (MD02-2518 and MD02-2519 DSRa*) are particularly valuable as they give us the opportunity to investigate in detail high- to low-latitude teleconnections in the Earth climate system over the last two glacial cycles (as opposed to the sole MIS 2–4) in addition to comparing records from the Atlantic with tropical Pacific.

3.2. Pacing of the Low-Latitude Millennial-Scale Events

In records from Greenland and the North Atlantic, the millennial-scale events show a dominant periodicity of the 1–2 ka cycle during glacial times with asymmetrical shapes between the warm and the cold phases [*Bond et al.*, 1999; *Grootes and Stuiver*, 1997; *Oppo et al.*, 1998; *van Kreveld et al.*, 2000]. In the records from NW Mexico, the spectral and wavelet analyses indicate similar periodicities (Figures 5 and 6). This is expected considering that the records were tuned to the GISP2 chronology. However, some differences also emerge. Although the 1–2 ka/cycle is identified in the cores MD02-2518 and MD02-2519 during the last glacial period, this periodicity is not dominant as in the high-latitude records [e.g., *Bond et al.*, 1999]. Instead, periodicities of ~5.4, 4.1, and 2.9 ka/cycle are stronger in the spectral and wavelets analyses during the last glacial (Figures 5c, 5d, and 6). Thus, given the >90% confidence associated with these cycles, they cannot be statistically dismissed as stochastically forced variations. In Figure 5e, the sum of three Gaussian band-pass filters is compared to the DSRa* record of Core MD02-2519. It shows that the combination of the periodical events every ~5.4, 4.1, and 2.9 ka/cycle can explain most of the changes in the records from the ETNP during the last glacial. The results of the spectral and wavelets analysis on the penultimate glacial period (MIS 6) also display some differences when compared to the last glacial period. Here the most consistent cycles occur every 6.7, 3.8, and 2.9 ka/cycle (Figure 5g). Although the periodicities at 3.8 and 2.9 ka cycle could be compared to those centered at 4.1 and 2.9 ka cycle during MIS 2–4, the dominant periodicity centered at 6.7 ka suggests less frequent millennial events in MIS 6 relative to the last glacial cycle (Figure 6).

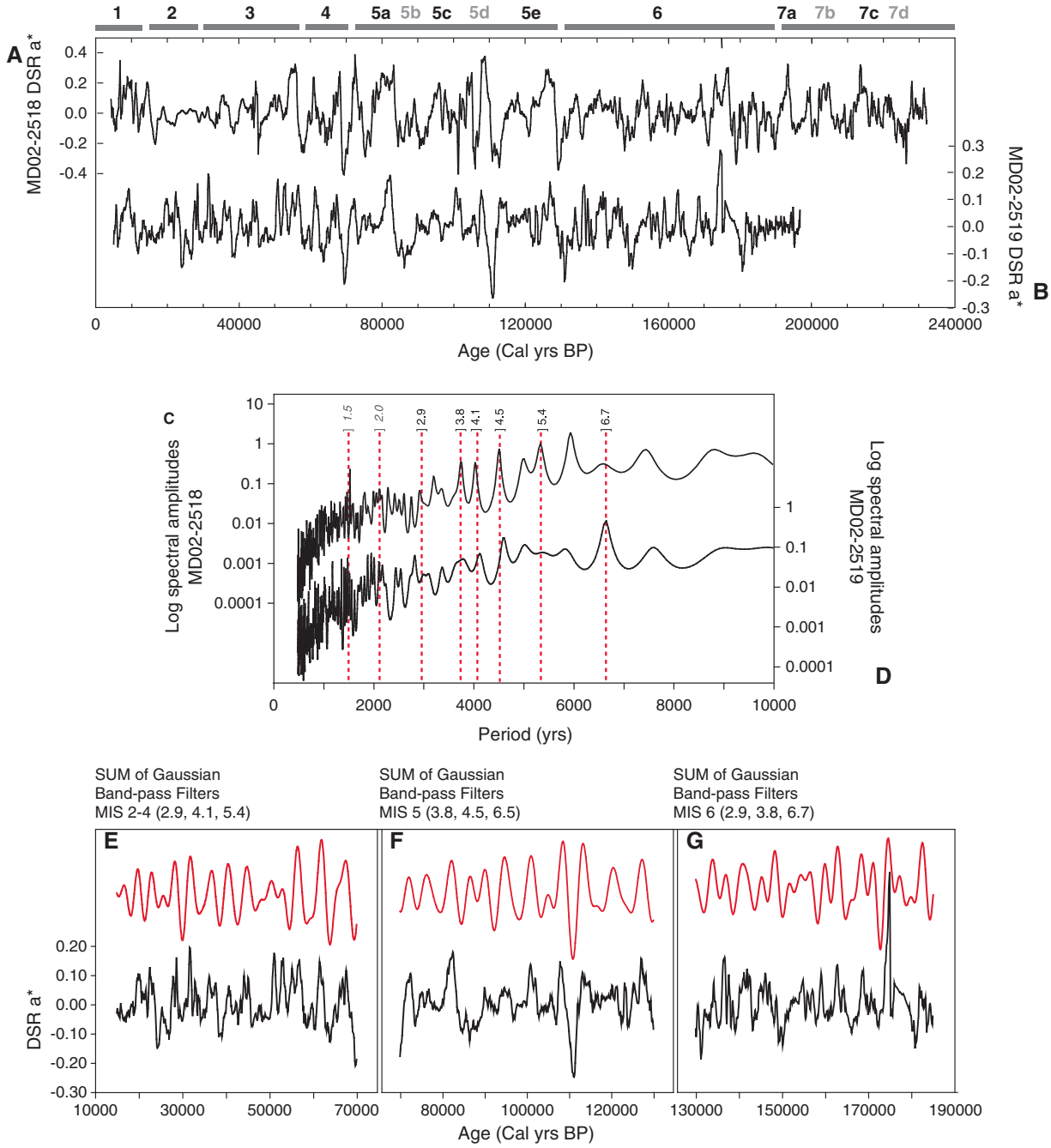

Figure 5. Spectral analyses applied to the DSRa* records (orbital trend removed) of cores (a) MD02-2518 and (b) MD02-2519. (c and d) The spectral results. The dotted red lines indicate the most prominent periodicities of the MIS 2–4, MIS 5, and MIS 6, where the black numbers are the main values and intervals of the periodicities for both records (including the "1–2 ka cycle"), later confirmed by the results of wavelets analyses (see Figure 6). Combined red lines are the SUM of Gaussian band-pass filters (bandwidth = 0.2×10^{-4}) between (e) 15 and 70 ka (MIS 2–4) with periodicities centered at 2.9, 4.1, and 5.4 ka (frequencies of 3.4×10^{-4}, 2.4×10^{-4}, and 1.85×10^{-4} cycles/yr, respectively). (f) Period between 70 and 130 ka (MIS 5) centered at 3.8, 4.5, and 6.5 ka (frequencies = 2.60×10^{-4}, 2.2×10^{-4}, and 1.55×10^{-4} cycles/yr, respectively). (e) Period between 130 and 185 ka (MIS 6) centered at 2.9, 3.8, and 6.7 ka (frequencies = 3.5×10^{-4}, 2.7×10^{-4}, and $1.5 \times 10 - 4$ cycles/yr, respectively). The comparison shows that most of the variability seen in the eastern tropical North Pacific records (black lines in Figures 5e–5g) can be explained by the sum of these cycles (red lines in Figures 5e–5g).

The spectral analyses for MIS 5 (Figure 5f) show dominant periodicities at 6.5, 4.5, and 3.8 ka cycle for both cores. Although the 1–2 ka/cycle is also present, it is not dominant. It is notable that the significance of the 1–2 ka cycle in the Greenland $\delta^{18}O$ records also decreases drastically during MIS 5 [*Bond et al.*, 1999]. In summary, our analysis reveals that low-frequency bands are more predominant, particularly in the older

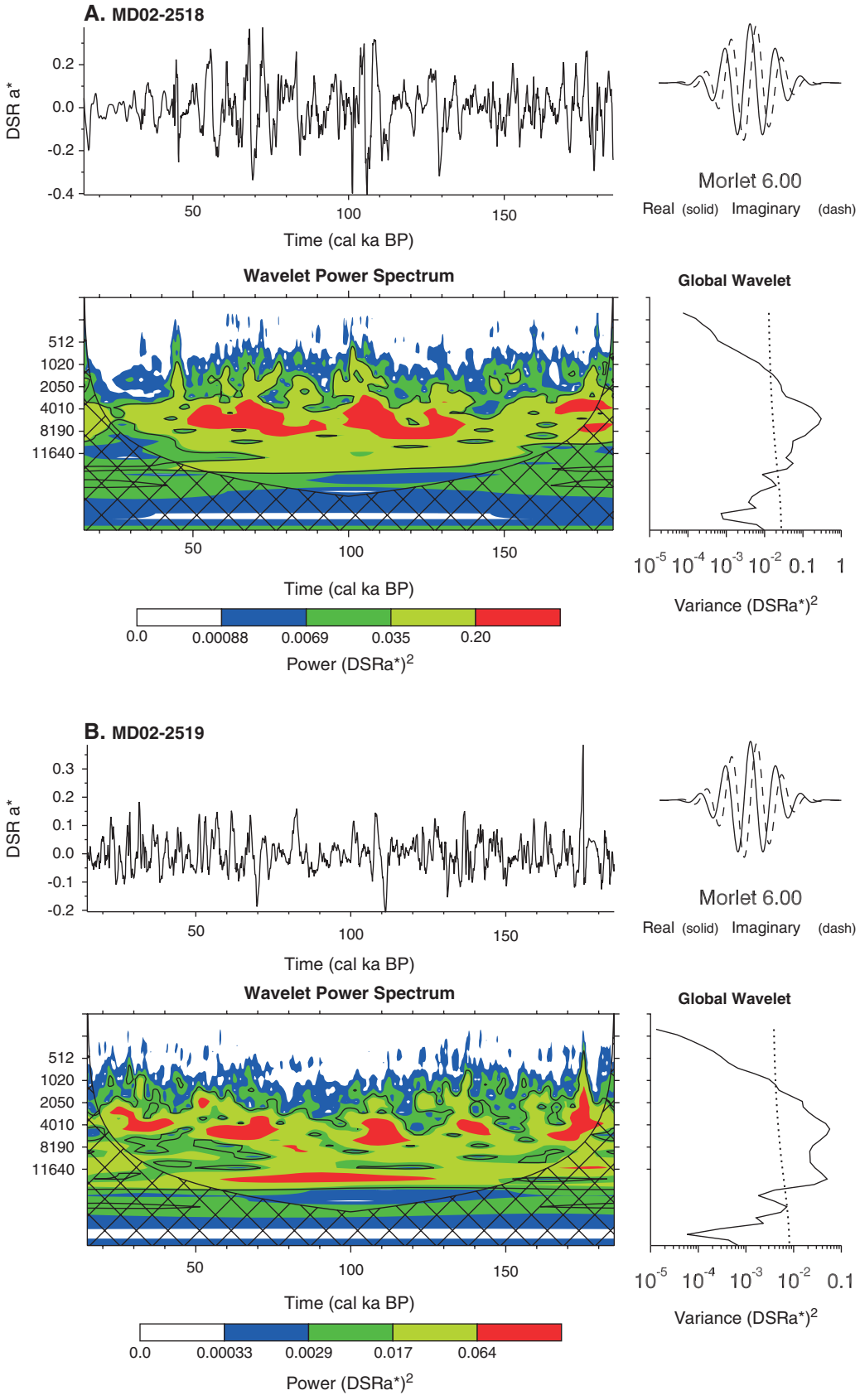
A. MD02-2518
DSR a*
0.2
0.0
-0.2
-0.4
50
100
150
Time (cal ka BP)
Morlet 6.00
Real (solid) Imaginary (dash)
Wavelet Power Spectrum
512
1020
2050
4010
8190
11640
Time (cal ka BP)
0.0
0.00088
0.0069
0.035
0.20
Power (DSRa*)2
Global Wavelet
10-5 10-4 10-3 10-2 0.1 1
Variance (DSRa*)2
B. MD02-2519
DSR a*
0.3
0.2
0.1
0.0
-0.1
-0.2
Time (cal ka BP)
Morlet 6.00
Real (solid) Imaginary (dash)
Wavelet Power Spectrum
Time (cal ka BP)
0.0
0.00033
0.0029
0.017
0.064
Power (DSRa*)2
Global Wavelet
10-5 10-4 10-3 10-2 0.1
Variance (DSRa*)2

Figure 6

Table 2. Comparison of the Dominant Periodicities (years/cycle) Over Different Time Slices (MIS), Among Millennial-Scale Records From High and Low Latitudes (See Main Text for References)

Record	MIS 2–4	MIS 5	MIS 6
MD02-2519 DSRa*	2900, 4100, 5300	3600, 4500, 6300	2900, 3800, 6700
Chinese speleothem $\delta^{18}O$	3300, 5000, 7700	3600, 5100, 7700	3000, 4900, 9000
EDC CH_4 record	2900, 4800, 6500	4400, 5400, 7100	3030, 5100, 8000
Greenland synthetic record	2900, 4900, 6600	3200, 4800, 6500	2400, 4300, 8000
ODP977A $\delta^{18}O$ Iberian Margin	1500, 3100, 5130	2500, 4600, 7400	2500, 3030, 4400

part of the records (6.5 ka and 6.7 ka/cycle in MIS 5 and MIS 6, respectively), suggesting a possible increase in frequency of millennial-scale events approaching the last glacial period (MIS 2).

4. Discussion

Our records suggest that millennial-scale climate variability has been persistent in the ETNP over the last two glacial-interglacial cycles. Detailed time series and wavelet analyses further reveal subtle differences during the penultimate glacial period (MIS 6) relative to the last glacial cycle (MIS 2–4). The key result of this study is the dominance of the low-frequency events in the older part of the record and the reduced significance of the 1–2 ka cycle in the ETNP climatic records over the last 240 ka B.P. Comparing these results from the tropical Pacific with other millennial-scale records spanning the middle to late Pleistocene period sheds further light on the nature of millennial-scale climate variability. Table 2 summarizes the dominant periodicity bands in these high and low-latitude records.

4.1. The Nature of Millennial-Scale Climate Variability During the Middle to Late Pleistocene

The reduced significance of the 1–2 ka/cycle documented in our records during the last glacial interval relative to the North Atlantic could be caused by the "symmetric pattern" displayed in the %OC and DSRa* records. In other words, the symmetrical shape could "smooth" two smaller periods into "one" more significant. Although this possibility cannot be completely eliminated, the reduced significance of the 1–2 ka/cycle has been reported in other millennial-scale records including the very high resolution Chinese speleothem record. Studies from midlatitude records off California and Oregon during the last glacial period have reported equivalent results to those found off NW Mexico, where periodicities longer than 3 ka are prominent over shorter ones [*Pisias et al.*, 2001]. Although these observations were originally interpreted as changes in the northward flow of the California Countercurrent [*Pisias*, 1978], of further significance was the suggestion that the NE Pacific reflects the response of the variability in the tropical Pacific [*Pisias et al.*, 2001]. Spectral and wavelet analyses from tropical records worldwide clearly denote the dominance of longer periodicities during the last glacial period. Data from stalagmites in Southern Africa report the strongest variability centered on periodicities between 2.5 and 4 ka [*Holmgrena et al.*, 2003]. Lake records from Tanzania indicate dominant periodicities at 3.6, 7.6, and 11.3 ka [*Garcin et al.*, 2006], similar to terrestrial reconstructions of surface moisture in NE Australia [*Turney et al.*, 2004]. Furthermore, results from the Cariaco Basin (Venezuela) and the SE Pacific (off Chile) show main periodicity bands centered at 4.5 and 3.1 ka, even though weaker periodicities (1–2 ka) are also present [*Kaiser et al.*, 2007]. Periodicities >5 ka have been recognized in the glacial North Atlantic records, although they have been related to Heinrich events occurring every 5 to 10 ka (~7.0 ± 2.4 ka) [*MacAyeal*, 1993; *McManus et al.*, 1999]. Hence, it is likely that the predominance of the longer periodicity bands (5.3, 4.1 and 2.9 ka cycle) relative to shorter ones is an essential feature of tropical climate variability at millennial scale worldwide (Table 2).

Figure 6. Wavelet analyses applied to DSRa* records between 15 and 185 ka B.P. (orbital trend removed) of cores (a) MD02-2518 and (b) MD02-2519. The wavelet power spectra analyses use the Morlet method (nondimensional frequency = 6). Contour levels are chosen so that 75%, 50%, 25%, and 5% of the wavelet power is above each level. Black contour is the 10% significance level, using a white noise background spectrum. The crosshatched region is the cone of influence (COI), where zero padding reduced the variance. The COI is the region of the wavelet spectrum defined as the *e*-folding time for the autocorrelation at each scale of the wavelet power. The *e*-folding time is chosen such that the wavelet power for a discontinuity at the edge drops by a factor of e^{-2} and ensures that edge effects are negligible beyond that point. The global wavelet power spectrum is shown in black line. The dashed line is the significance (variance) for the global wavelet spectrum, assuming the same significance level and background spectrum as in the contour plot [*Torrence and Compo*, 1998].

Moreover, the less frequent millennial-scale variability over MIS 6 relative to MIS 2–4 has been previously noted in both the Northern and Southern Hemispheres. *Martrat et al.* [2004] documented the weaken of the 1–2 ka cycle in North Atlantic midlatitude records (i.e., Iberian Margin) and suggested that this frequency cycle is not a persistent characteristic of the climate system beyond the glacial period (Table 2). Indeed, IRD-events are reported to be less frequent during MIS 6 in the North Atlantic high latitudes [*McManus et al.*, 1999], indicating less frequent variability in the internal dynamics of the ice sheets (relative to MIS 2–4) in agreement with δ^{18}O-PF records (i.e., ODP-980) [*McManus et al.*, 1999]. Furthermore, this finding extends to records from Antarctica, where periods of ~10.0, 6.0, and 3.3 are dominant in Vostok δD, and CH_4 records during MIS 6 [*Siddall et al.*, 2006]. Thus, it seems that the preponderance of the 1–2 ka variability has only a limited expression confined the North Atlantic during the last glacial period. Therefore, this mode of variability cannot be regarded as a ubiquitous characteristic of millennial-scale climate system. In contrast, the increased predominance of low-frequency variability during MIS 5 and MIS 6 relative the last glacial period (MIS 2–4) seems to be a common characteristic of the climate records.

The persistence of millennial variability during MIS 6 in our records, when typical Heinrich events are less common in the North Atlantic [e.g., *Hemming*, 2004; *McManus et al.*, 1999], suggests that the millennial-scale climate variability is less dependent of ice sheet dynamics and the influx of ice armadas into the North Atlantic as previously thought [*Clark et al.*, 2002]. In contrast, the AMOC variability, which is thought to be the main trigger for the bipolar seesaw mechanism, persisted throughout the penultimate glacial period [*Margari et al.*, 2010], albeit with low-frequency events being more dominant [e.g., *Martrat et al.*, 2004]. Recent evidence from foraminiferal isotope and pollen records suggests wetter conditions in the North Atlantic stadial periods during MIS 6 which could have provided continuous freshwater discharge and effectively trigger the gradual deterioration of climate by slowly pushing the ocean circulation in the North Atlantic toward a threshold shutting of the AMOC [*Margari et al.*, 2010; *Martrat et al.*, 2007]. Additionally, wetter conditions also require less ice input to cause disruption in AMOC (i.e., smaller disruption threshold). AMOC can also equally respond to other factors such as variations of the Indo-Atlantic salinity exchange via the Agulhas salt leakage, for instance [*Marino et al.*, 2013]. Therefore, freshwater input from ice sheet calving may not be the essential prerequisite for AMOC changes and the global propagation of this climate signal at millennial scales. This conclusion is in line with recent studies, where ice sheet calving in the North Atlantic is thought as a response of DO stadials, rather than the trigger operating only during climatic transitions and periods of intermediate ice volume [*Barker et al.*, 2011; *Siddall et al.*, 2010].

Finally, Figure 7 and Table 2 provide a comparative summary of the climate records discussed in this study covering the last two glacial cycles. The reconstructed high-latitude Greenland temperature records (Figure 7a) [*Barker et al.*, 2011] show an increase during interstadials and decrease during stadials, a pattern similar to midlatitudes North Atlantic SST reflecting AMOC perturbation and bipolar seesaw (Figure 7b) [*Martrat et al.*, 2007]. The frequency of variability seen in the ETNP (Figures 7e and 7f) also appears to be remarkably similar to those found in the atmospheric concentration records CH_4, which is mainly emitted from NH tropical wetlands, suggesting large-scale changes in the hydrological cycle [*Loulergue et al.*, 2008], and possibly influenced by the position of the ITCZ over Northern Hemisphere continental land masses. Changes in monsoon intensity (Figures 7c and 7d) [e.g., *Wang et al.*, 2008b; *Wang et al.*, 2001] shows comparable pattern to the ETNP changes in export productivity driven by upwelling. Table 2 summarizes the dominant frequency band in high and low-latitude records. Interestingly, the summary reveals that the decrease in frequency of millennial cycles in the older part of the records is common feature while 1–2 ka/cycle is not significant with the exception of the last glacial period in the Iberian Margin MIS 2–4. This suggests a global expression of this mode of climate variability with relatively uniform pacing worldwide. Changes in the millennial-scale climate variability over time showing frequency increases approaching last climate cycle are also a common feature in middle to late Pliocene period, suggesting the ubiquitous nature of this trend. These considerations strongly suggest that the myriad of changes such as the AMOC, the atmospheric circulation, the bipolar seesaw, the latitudinal heat distribution, the position of the ITCZ, the hydrological cycle, and the GHG concentrations are highly coupled oceanic and atmospheric processes, playing a pivotal role in amplifying millennial-scale oscillations on a global scale. Thus, the most pertinent question in this regard is how the variability recorded in the tropical Pacific records fits in the picture of global teleconnections.

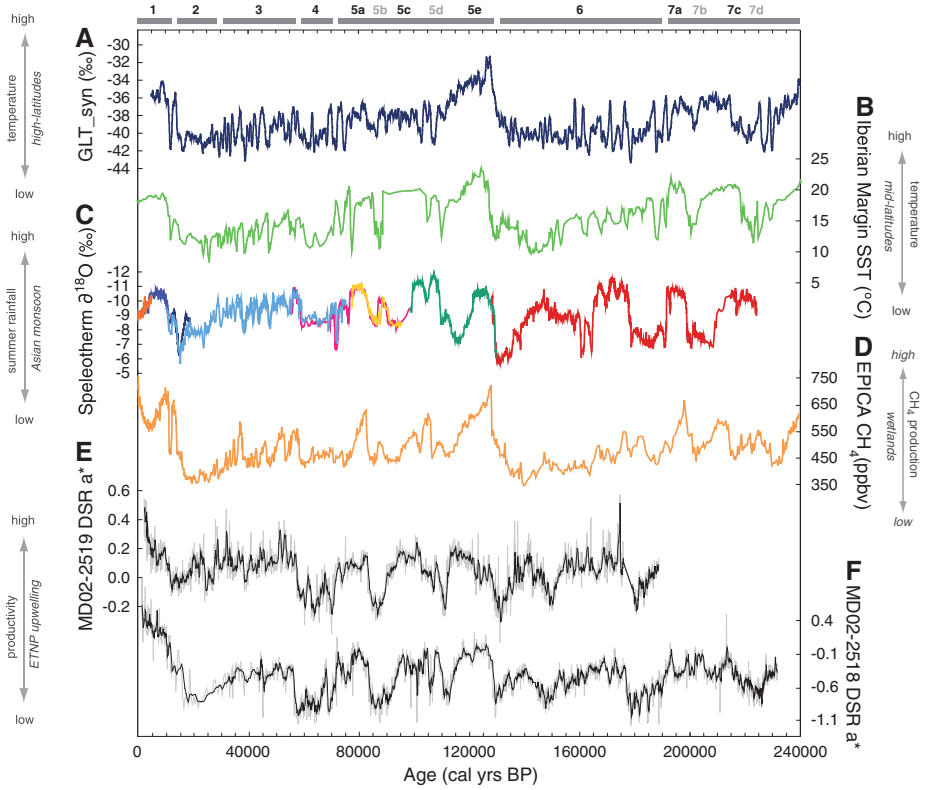

Figure 7. Comparison of millennial-scale climate variability reconstructed proxy records of temperature, greenhouse gasses, upwelling, and productivity over the last two glacial cycles. (a) Greenland temperature synthetic record (GLT_syn) (‰) [*Barker et al.*, 2011]; (b) ODP-977A Uk'37-record of SST (°C) [*Martrat et al.*, 2007]; (c) Speleothems Sanbao/Hulu $\delta^{18}O$ records [*Wang et al.*, 2008a] (red, stalagmite SB11; green, SB23; yellow, SB25-1; pink, SB22; dark blue, SB3; purple, SB10; and orange, SB26) and blue, Hulu cave [*Wang et al.*, 2001]; (d) CH4 from EPICA (using gas age EDC3) [*Loulergue et al.*, 2008]; (e) DSRa* of Core MD02-2519; and (f) DSRa* of Core MD02-2518. The synthetic Greenland $\delta^{18}O$ record is associated to high-latitude temperature variations, the Uk'37 record is associated to SST in the North Atlantic midlatitudes. The Chinese speleothem $\delta^{18}O$ record represents the Asian monsoon variability. The CH_4 record highlights large-scale changes in hydrological cycle and/or the position of the ITCZ, and the associated changes in the strength of tropical CH_4 sources and sinks. The ETNP DSRa* records represent sedimentary OC variations controlled by changes in productivity and wind-driven upwelling.

4.2. Millennial-Scale Oscillation in the Tropical Pacific as Part of the Global Teleconnections

In the ETNP records, the pattern of increase in %OC and its proxy record DSRa* during interstadials, and the decrease during stadials, has been found along the NE Pacific using a range of other productivity proxies. Thus, suggesting that these changes are related to upwelling and productivity in the California Current region during the Pleistocene [*Arellano-Torres et al.*, 2011; *Cartapanis et al.*, 2014; *Hendy et al.*, 2004; *McClymont et al.*, 2012; *White et al.*, 2013]. Denitrification and oxygen depletion in intermediate waters [*Cartapanis et al.*, 2011; *Chang et al.*, 2008; *Pichevin et al.*, 2010] have decreased/increased in parallel during stadials/interstadials along the entire western American margin from Canada to Costa Rica. This implies a unified or comparable response of the various upwelling cells and ventilation of intermediate waters distributed along the margin at millennial scale. This pattern can be explained through AMOC perturbations causing changes in latitudinal thermal gradients (the bipolar seesaw), which in turn causes latitudinal shifts in the ITCZ/monsoon systems and in the surface circulation. The mean position and the strength of Subtropical High are sensitive to latitudinal shifts ITCZ. A northward shift in the ITCZ should increase the meridional temperature gradients and strengthen the Subtropical High. Such changes in turn cause parallel changes in the upwelling strength, the biological production, and the intermediate water oxygen consumption [*Chiang*, 2009]. Globally, several studies indeed show evidences for a southward (northward) shift of the Pacific ITCZ during cold stadial (warm interstadial) episodes [*Koutavas and Lynch-Stieglitz*, 2004; *Leduc et al.*, 2009; *Peterson et al.*, 2000; *Wang et al.*, 2007]. Along the eastern Pacific, it consequently affects

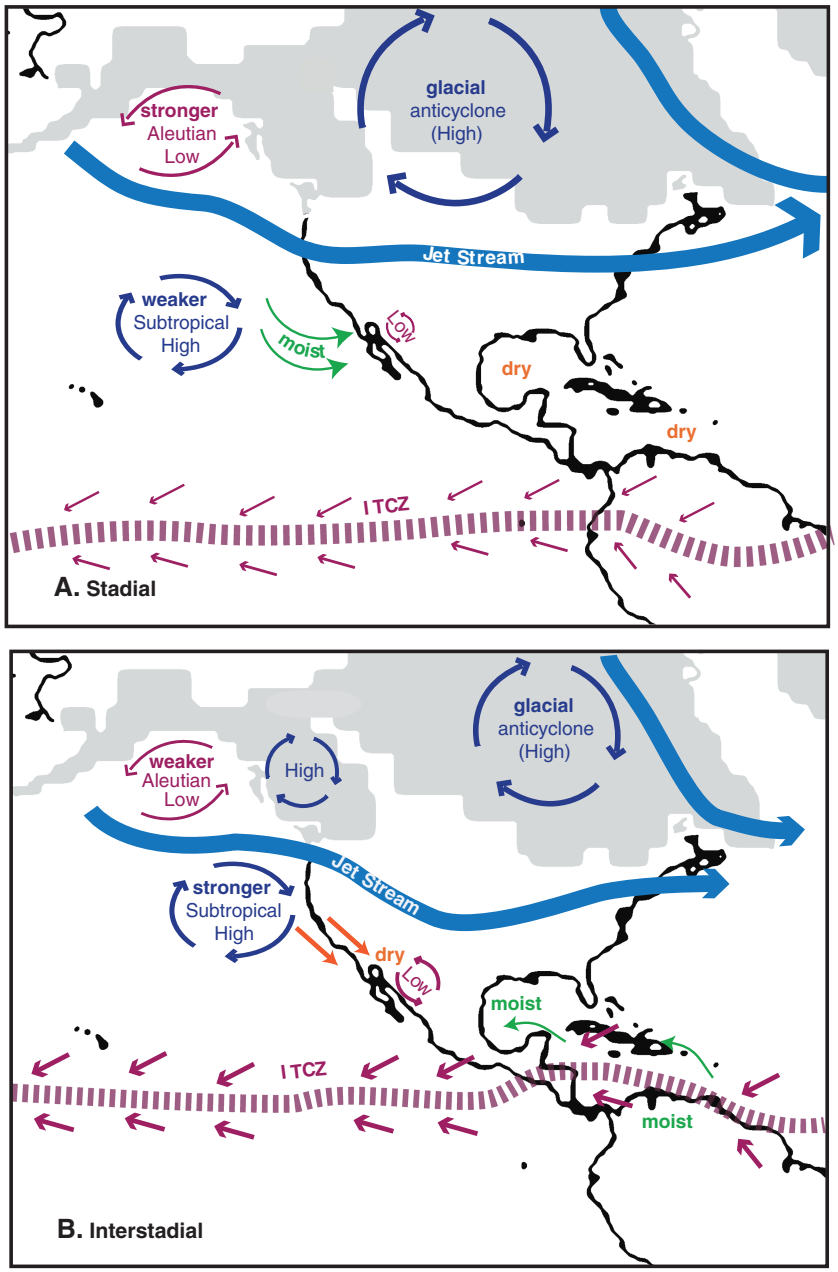

Figure 8. Schematic model of the proposed atmospheric circulation pattern occurred during (a) stadials and (b) interstadials over the last glacial. Aleutian Low, subpolar Aleutian Low pressure cell. Subtropical High, subtropical North Pacific High pressure cell. Low, Mexican Low pressure cell. ITCZ, marks an average latitudinal position of the Intertropical Convergence Zone. Green arrows show flow of ocean moist to land. Orange arrows are dry shore-parallel winds. Purple arrows are trade winds.

the intensity of the OMZ via varying oxidant demand in the subsurface, with impacts on GHG concentrations and global temperatures [*Hendy et al.*, 2002; *Hendy and Kennett*, 2003; *Ivanochko et al.*, 2005; *Vellinga and Wood*, 2002]. Independently, modeling studies imply that abrupt climate changes in the eastern Pacific can be forced directly from changes in AMOC and merely transported to the low latitudes via thermocline waters. In this scenario, more/less oxygen and nutrient-rich/poor conditions in the thermocline waters could cause both productivity and intermediate water oxygenation changes [*Schmittner and Galbraith*, 2008].

Although many of the scenarios outlined above regard AMOC changes as the underlying mechanism that globally amplifies millennial-scale variability through numerous atmospheric and oceanic teleconnection

processes, AMOC changes itself require concomitant changes in the hydrological cycle [*Chiang*, 2009]. This is particularly relevant to the penultimate glacial period, when typical Heinrich ice sheet calving events appear to be absent in the North Atlantic records [*Hemming*, 2004; *Margari et al.*, 2010; *Martrat et al.*, 2007]. We argue that this highlights the tight coupling between the teleconnection processes that amplify the climate system at millennial scale.

In Figure 8, we propose a schematic reconstruction that illustrates the atmospheric reorganization, reflecting the contrasting condition in the ETNP during both stadial and interstadial periods (Figures 8a and 8b). This takes into account evidence from proxy records as well as climate model results [*Hendy and Kennett,* 1999, 2000; *Metcalfe et al.*, 2002, 2000; *Ortega-Guerrero et al.*, 1999; *Peltier*, 1994; *Peterson et al.*, 2000; *Stott et al.*, 2002; *van Meerbeeck et al.*, 2009]. Relative to the modern scenario (see Figure 1), the presence of the Laurentide ice sheet leads to a semipermanent glacial anticyclonic High on land and restricts the seasonal latitudinal migration of the subtropical High; however, its intensity is sensitive to the meridional temperature gradients generated by the seasonal migration of the ITCZ. We propose that during interstadials, when productivity and thermocline oxygen depletion were high in the ETNP, the ITCZ was shifted to a northward position. This increased the subtropical temperature gradients resulting in a more intense subtropical High associated with a weaker Aleutian Low and the onshore location of Mexican Low on the NW Mexican mainland [*Ganeshram and Pedersen*, 1998]. Such atmospheric configuration is conducive for shore-parallel winds driving strong upwelling in the California Current region. According to coupled climate model simulations, a stronger subtropical High of this configuration could enhance summer wind-driven upwelling during the interstadials [*McClymont et al.*, 2012]. Conversely, during stadials the southward retreat of the ITCZ in response to changes in interhemispheric thermal gradients [*Peterson et al.*, 2000] reduced the strength of the subtropical High. This decreased the shore-parallel winds [*McClymont et al.*, 2012], reducing upwelling and productivity and increasing water column oxygenation along the NE Pacific [*Cheshire et al.*, 2005; *Hendy and Kennett,* 1999, 2000]. This scenario depicted in Figure 8 also takes into account changes in wet/dry conditions in response to the position of ITCZ and the resultant changes in moisture sources, as recorded on Mexican mainland reconstructions [*Metcalfe et al.*, 2002, 2000; *Ortega-Guerrero et al.*, 1999] This is consistent with uniform and large-scale millennial-scale variations in the ETNP upwelling strength and the California Current region associated with millennial-scale climate variability [*Arellano-Torres et al.*, 2011; *McClymont et al.*, 2012].

5. Conclusions

1. Two continuous records of paleoproductivity changes from the ETNP spanning the last ~ 240 ka B.P. show the persistence millennial-scale changes in productivity over the last two glacial-interglacial cycles in the tropical Pacific spanning the middle to late Pleistocene.
2. The spectral and wavelet analysis reveal the predominance of low-frequency events and an increase in the frequency of millennial-scale events from MIS 6 approaching the last glacial period (MIS 2).
3. The persistence of millennial-scale variations during the penultimate glacial period in the absence of typical Heinrich ice rafting events suggests that the ice sheet calving may not be an essential prerequisite for millennial-scale climate variability.
4. Given the remarkable similarity in the pacing of millennial-scale record worldwide over long time periods, we suggest that the pacing of the millennial-scale climate variability may represent a natural resonance inherent to the climate system, amplified by tightly coupled oceanic and atmospheric teleconnection processes.
5. We use schematic reconstruction to argue that atmospheric reorganization in the NE Pacific climate during millennial stadial and interstadial periods is consistent with scenarios of tightly coupled global teleconnection processes involving AMOC perturbations, changes in interhemispheric thermal gradients, the shift in ITCZ position, and the strength of the subtropical North Pacific High.

Acknowledgments

Details for age model construction are included in the supporting information. Data for this paper are provided in the Data Set S1. This study was funded by a NERC standard grant and a European Science Foundation grant awarded to R.S.G. We are thankful to the staff and crew of RV *Marion Dufresne* for coring support through IMAGES IV programme. E.A.T. is grateful to the ORSAS Scholarship scheme that supported her study at the School of Geosciences, the University of Edinburgh. Radiocarbon dating was conducted through NERC RCL allocations 1132.0405 (Core MD02-2518) and 1259.1007 (MD02-2519). We thank to Steve Moreton (NERC RCL) for his help with radiocarbon dating and Colin Chilcott for CN and stable isotope analyses. All authors are grateful to the Editor and two anonymous reviewers for the comments and corrections made to improve this paper.

References

Altabet, M. A., M. J. Higginson, and D. W. Murray (2002), The effect of millennial-scale changes in Arabian Sea denitrification on atmospheric CO_2, *Nature*, *415*(6868), 159–162.

Arellano-Torres, E., L. E. Pichevin, and R. S. Ganeshram (2011), High-resolution opal records from the eastern tropical Pacific provide evidence for silicic acid leakage from HNLC regions during glacial periods, *Quat. Sci. Rev.*, *30*(9–10), 1112–1121.

Badan-Dangon, A. (1998), Coastal circulation from the Galápagos to the Gulf of California, in *The Sea*, vol. 11, edited by A. R. Robinson and K. H. Brink, pp. 315–344, John Wiley, New York.

Bakun, A., and C. S. Nelson (1991), The seasonal cycle of wind stress curl in subtropical eastern boundary current regions, *J. Phys. Oceanogr.*, *21*, 1815–1834.
Barker, S., G. Knorr, R. L. Edwards, F. Parrenin, A. E. Putnam, L. C. Skinner, E. Wolff, and M. Ziegler (2011), 800,000 years of abrupt climate variability, *Science*, *334*(6054), 347–351.
Bar-Matthews, M., A. Ayalon, M. Gilmour, A. Matthews, and C. J. Hawkesworth (2003), Sea-land oxygen isotopic relationships from planktonic foraminifera and speleothems in the Eastern Mediterranean region and their implication for paleorainfall during interglacial intervals, *Geochim. Cosmochim. Acta*, *67*(17), 3181–3199.
Barry, R. G., and R. J. Chorley (2003), *Atmosphere, Weather and Climate*, Routledge, New York.
Beaufort, L. (2002), IMAGES VIII MONA Cruise Report, in *Institut Polaire Francais Paul-Émile Victor (IPEV), les rapports de campagnes à la mer*, edited, p. 452, PANGAEA. [Available at http://www.images-pages.org/ftp/pub/MONA/MONA_cruise_report.pdf.]
Behl, R. J., and J. P. Kennett (1996), Brief interstadial events in the Santa Barbara basin, NE Pacific, during the past 60 kyr, *Nature*, *379*(6562), 243–246.
Blunier, T., et al. (1998), Asynchrony of Antarctic and Greenland climate change during the last glacial period, *Nature*, *394*(6695), 739–743.
Bond, G. C., W. Showers, M. Elliot, M. Evans, R. Lotti, I. Hajdas, G. Bonani, and S. Johnson (1999), The North Atlantic's 1–2 kyr climate rhythm: Relation to Heinrich events, Dansgaard/Oeschger cycles and the little ice age, in *Mechanisms of Global Change at Millennial Time Scales*, edited by P. U. Clark, R. S. Webb, and L. D. Keigwin, pp. 59–76, AGU, Washington, D. C.
Bond, G., W. Broecker, S. Johnsen, J. McManus, L. Labeyrie, J. Jouzel, and G. Bonani (1993), Correlations between climate records from North-Atlantic sediments and Greenland ice, *Nature*, *365*(6442), 143–147.
Brandes, J. A., A. H. Devol, T. Yoshinari, D. A. Jayakumar, and S. W. A. Naqvi (1998), Isotopic composition of nitrate in the central Arabian Sea and eastern tropical North Pacific: A tracer for mixing and nitrogen cycles, *Limnol. Oceanogr.*, *43*(7), 1680–1689.
Broecker, W. S. (1992), The Great Ocean Conveyor, *Global Warming Phys. Fact.*, *247*, 129–161.
Cane, M. A. (1998), Climate change—A role for the tropical Pacific, *Science*, *282*(5386), 59.
Cannariato, K. G., J. P. Kennett, and R. J. Behl (1999), Biotic response to late Quaternary rapid climate switches in Santa Barbara Basin: Ecological and evolutionary implications, *Geology*, *27*, 63–66.
Cartapanis, O., K. Tachikawa, and E. Bard (2011), Northeastern Pacific oxygen minimum zone variability over the past 70 kyr: Impact of biological production and oceanic ventilation, *Paleoceanography*, *26*, PA4208, doi:10.1029/2011PA002126.
Cartapanis, O., K. Tachikawa, O. E. Romero, and E. Bard (2014), Persistent millennial-scale link between Greenland climate and northern Pacific oxygen minimum zone under interglacial conditions, *Clim. Past Discuss.*, *9*(4), 3919–3952.
Chang, A. S., T. F. Pedersen, and I. L. Hendy (2008), Late Quaternary paleoproductivity history on the Vancouver Island margin, western Canada: A multiproxy geochemical study, *Can. J. Earth Sci.*, *45*(11), 1283–1297.
Cheshire, H., J. Thurow, and A. J. Nederbragt (2005), Late Quaternary climate change record from two long sediment cores from Guaymas Basin, Gulf of California, *J. Quaternary Sci.*, *20*(5), 457–469.
Chiang, J. C. H. (2009), The tropics in paleoclimate, in *Annual Review of Earth and Planetary Sciences*, vol. 37, edited by R. Jeanloz and K. H. Freeman, pp. 263–297, Annu. Revs. Palo Alto, Calif.
Clark, P. U., N. G. Pisias, T. F. Stocker, and A. J. Weaver (2002), The role of the thermohaline circulation in abrupt climate change, *Nature*, *415*(6874), 863–869.
Clement, A. C., R. Seager, and M. A. Cane (1999), Orbital controls on the El Nino/Southern Oscillation and the tropical climate, *Paleoceanography*, *14*(4), 441–456, doi:10.1029/1999PA900013.
Crowley, T. J. (1992), North Atlantic Deep Water cools the southern hemisphere, *Paleoceanography*, *7*(4), 489–497, doi:10.1029/92PA01058.
Curry, W., and D. W. Oppo (1997), Synchronous, high frequency oscillations in the tropical sea surface temperature and North Atlantic deep-water production during the last glacial cycle, *Paleoceanography*, *12*, 1–14, doi:10.1029/96PA02413.
Dansgaard, W., S. J. Johnsen, H. B. Clausen, D. Dahl-Jensen, N. Gundestrup, C. U. Hammer, and H. Oeschger (1984), North Atlantic climatic oscillations revealed by deep Greenland ice cores, in *Climatic Processes and Climate Sensitivity*, *Geophys. Monogr. Ser.*, edited by J. E. Hansen and T. Takahashi, pp. 288–298, AGU, Washington, D. C.
Dansgaard, W., et al. (1993), Evidence for general instability of past climate from a 250-kyr ice-core record, *Nature*, *364*, 218–220.
Emmer, E., and R. C. Thunell (2000), Nitrogen isotope variations in Santa Barbara Basin sediments: Implications for denitrification in the eastern tropical North Pacific during the last 50,000 years, *Paleoceanography*, *15*(4), 377–387, doi:10.1029/1999PA000417.
Flückiger, J., A. Dallenbach, T. Blunier, B. Stauffer, T. F. Stocker, J. M. Raynaud, and J. M. Barnola (1999), Variations in atmospheric N_2O concentration during abrupt climatic changes, *Science*, *285*, 227–230.
Flückiger, J., T. Blunier, B. Stauffer, J. Chappellaz, R. Spahni, K. Kawamura, J. Schwander, T. F. Stocker, and D. Dahl-Jensen (2004), N_2O and CH_4 variations during the last glacial epoch: Insight into global processes, *Global Biogeochem. Cycles*, *18*, GB1020, doi:10.1029/2003GB002122.
Ganeshram, R. S., and T. F. Pedersen (1998), Glacial-interglacial variability in upwelling and bioproductivity off NW Mexico: Implications for quaternary paleoclimate, *Paleoceanography*, *13*(6), 634–645, doi:10.1029/98PA02508.
Ganeshram, R. S., T. F. Pedersen, S. E. Calvert, and J. W. Murray (1995), Large changes in oceanic nutrient inventories from glacial to interglacial periods, *Nature*, *376*(6543), 755–758.
Ganeshram, R. S., S. E. Calvert, T. F. Pedersen, and G. L. Cowie (1999), Factors controlling the burial of organic carbon in laminated and bioturbated sediments off NW Mexico: Implications for hydrocarbon preservation, *Geochim. Cosmochim. Acta*, *63*(11–12), 1723–1734.
Ganeshram, R. S., T. F. Pedersen, S. E. Calvert, G. W. McNeill, and M. R. Fontugne (2000), Glacial-interglacial variability in denitrification in the World's Oceans: Causes and consequences, *Paleoceanography*, *15*(4), 361–376, doi:10.1029/1999PA000422.
Garcin, Y., D. Williamson, M. Taieb, A. Vincens, P. E. Mathé, and A. Majule (2006), Centennial to millennial changes in maar-lake deposition during the last 45,000 years in tropical Southern Africa (Lake Masoko, Tanzania), *Palaeogeogr. Palaeoclimatol. Palaeoecol.*, *239*, 334–354.
Grootes, P. M., and M. Stuiver (1997), Oxygen 18/16 variability in Greenland snow and ice with 10(-3)- to 10(5)-year time resolution, *J. Geophys. Res.*, *102*(C12), 26,455–26,470, doi:10.1029/97JC00880.
Haug, G. H., K. A. Hughen, D. M. Sigman, L. C. Peterson, and U. Rohl (2001), Southward migration of the intertropical convergence zone through the Holocene, *Science*, *293*(5533), 1304–1308.
Heinrich, H. (1988), Origin and consequences of cycling ice rafting in the Northeast Atlantic Ocean during the past 130,000 years, *Quat. Res.*, *29*, 142–152.
Hemming, S. R. (2004), Heinrich events: Massive late Pleistocene detritus layers of the North Atlantic and their global climate imprint, *Rev. Geophys.*, *42*, RG1005, doi:10.1029/2003RG000128.
Hendy, I. L., and J. P. Kennett (1999), Latest Quaternary North Pacific surface-water responses imply atmosphere-driven climate instability, *Geology*, *27*(4), 291–294.

Hendy, I. L., and J. P. Kennett (2000), Dansgaard-Oeschger cycles and the California Current System: Planktonic foraminiferal response to rapid climate change in Santa Barbara Basin, Ocean Drilling Program hole 893A, *Paleoceanography*, *15*(1), 30–42, doi:10.1029/1999PA000413.
Hendy, I. L., and J. P. Kennett (2003), Tropical forcing of North Pacific intermediate water distribution during Late Quaternary rapid climate change?, *Quat. Sci. Rev.*, *22*(5–7), 673–689.
Hendy, I. L., and T. F. Pedersen (2005), Is pore water oxygen content decoupled from productivity on the California Margin? Trace element results from Ocean Drilling Program Hole 1017E, San Lucia slope, California, *Paleoceanography*, *20*, PA4026, doi:10.1029/2004PA001123.
Hendy, I. L., J. P. Kennett, E. B. Roark, and B. L. Ingram (2002), Apparent synchroneity of submillennial scale climate events between Greenland and Santa Barbara Basin, California from 30-10 ka, *Quat. Sci. Rev.*, *21*(10), 1167–1184.
Hendy, I. L., T. F. Pedersen, J. P. Kennett, and R. Tada (2004), Intermittent existence of a southern Californian upwelling cell during submillennial climate change of the last 60 kyr, *Paleoceanography*, *19*, PA3007, doi:10.1029/2003PA000965.
Holmgrena, K., J. A. Lee-Thorpb, G. R. J. Cooperc, K. Lundblada, T. C. Partridged, L. Scotte, R. Sithaldeenb, A. S. Talmaf, and P. D. Tyson (2003), Persistent millennial-scale climatic variability over the past 25,000 years in Southern Africa, *Quat. Sci. Rev.*, *22*, 2311–2326.
Intergovernmental Panel on Climate Change (2007), *Climate Change 2007: The Physical Science Basis. Contribution of Working Group I to the Fourth Assessment Report of the Intergovernmental Panel on Climate Change, 2007*, Cambridge Univ. Press, Cambridge, U. K., and New York.
Ivanochko, T. S., R. S. Ganeshram, G. J. A. Brummer, G. Ganssen, S. J. A. Jung, S. G. Moreton, and D. Kroon (2005), Variations in tropical convection as an amplifier of global climate change at the millennial scale, *Earth Planet. Sci. Lett.*, *235*(1–2), 302–314.
Kaiser, J., F. Lamy, H. W. Arz, and D. Hebbeln (2007), Dynamics of the millennial-scale sea surface temperature and Patagonian ice sheet fluctuations in southern Chile during the last 70 kyr (ODP Site 1233), *Quat. Int.*, *161*, 77–89.
Keigwin, L. D., and G. A. Jones (1994), Western North-Atlantic evidence for millennial-scale changes in ocean circulation and climate, *J. Geophys. Res.*, *99*(C6), 12,397–12,410, doi:10.1029/94JC00525.
Kennett, J. P., and B. L. Ingram (1995), A 20,000-year record of ocean circulation and climate change from the Santa Barbara Basin, *Nature*, *377*, 510–512.
Kessler, W. S. (2006), The circulation of the eastern tropical Pacific: A review, *Prog. Oceanogr.*, *69*(2–4), 181–217.
Koutavas, A., and J. Lynch-Stieglitz (2004), Variability of the marine ITCZ over the eastern Pacific during the past 30,000 years—Regional perspective and global context, *Hadley Circulation Present Past Future*, *21*, 347–369.
Koutavas, A., J. Lynch-Stieglitz, T. M. Marchitto, and J. P. Sachs (2002), El Nino-like pattern in ice age tropical Pacific sea surface temperature, *Science*, *297*(5579), 226–230.
Kutzbach, J., R. Gallimore, S. Harrison, P. Behling, R. Selin, and F. Laarif (1998), Climate and biome simulations for the past 21,000 years, *Quat. Sci. Rev.*, *17*(6–7), 473–506.
Lavin, M. F., G. Gaxiolacastro, J. M. Robles, and K. Richter (1995), Winter water masses and nutrients in the northern Gulf of California, *J. Geophys. Res.*, *100*(C5), 8587–8605, doi:10.1029/95JC00138.
Leduc, G., L. Vidal, K. Tachikawa, and E. Bard (2009), ITCZ rather than ENSO signature for abrupt climate changes across the tropical Pacific?, *Quat. Res.*, *72*(1), 123–131.
Loulergue, L., A. Schilt, R. Spahni, V. Masson-Delmotte, T. Blunier, B. Lemieux, J.-M. Barnola, D. Raynaud, T. F. Stocker, and J. Chappellaz (2008), Orbital and millennial-scale features of atmospheric CH4 over the past 800,000 years, *Nature*, *453*(7193), 383–386.
MacAyeal, D. R. (1993), Binge/purge oscillations of the Laurentide ice sheet as a cause of the North Atlantic's Heinrich events, *Paleoceanography*, *8*(6), 775–784, doi:10.1029/93PA02200.
Margari, V., L. C. Skinner, P. C. Tzedakis, A. Ganopolski, M. Vautravers, and N. J. Shackleton (2010), The nature of millennial-scale climate variability during the past two glacial periods, *Nat. Geosci.*, *3*(2), 127–131.
Marino, G., R. Zahn, M. Ziegler, C. Purcell, G. Knorr, I. R. Hall, P. Ziveri, and H. Elderfield (2013), Agulhas salt-leakage oscillations during abrupt climate changes of the Late Pleistocene, *Paleoceanography*, *28*, 599–606, doi:10.1002/palo.20038.
Martrat, B., J. O. Grimalt, C. Lopez-Martinez, I. Cacho, F. J. Sierro, J. A. Flores, R. Zahn, M. Canals, J. H. Curtis, and D. A. Hodell (2004), Abrupt temperature changes in the Western Mediterranean over the past 250,000 years, *Science*, *306*(5702), 1762–1765.
Martrat, B., J. O. Grimalt, N. J. Shackleton, L. de Abreu, M. A. Hutterli, and T. F. Stocker (2007), Four climate cycles of recurring deep and surface water destabilizations on the Iberian margin, *Science*, *317*(5837), 502–507.
McClymont, E. L., R. S. Ganeshram, L. E. Pichevin, H. M. Talbot, B. E. van Dongen, R. C. Thunell, A. M. Haywood, J. S. Singarayer, and P. J. Valdes (2012), Sea-surface temperature records of Termination 1 in the Gulf of California: Challenges for seasonal and interannual analogues of tropical Pacific climate change, *Paleoceanography*, *27*, PA2202, doi:10.1029/2011PA002226.
McManus, J. F., D. W. Oppo, and J. L. Cullen (1999), A 0.5-million-year record of millennial-scale climate variability in the North Atlantic, *Science*, *283*(5404), 971–975.
Metcalfe, S. E., S. L. O'Hara, M. Caballero, and S. J. Davies (2000), Records of Late Pleistocene-Holocene climatic change in Mexico—A review, *Quat. Sci. Rev.*, *19*(7), 699–721.
Metcalfe, S., A. Say, S. Black, R. McCulloch, and S. O'Hara (2002), Wet conditions during the last glaciation in the Chihuahuan Desert, Alta Babicora Basin, Mexico, *Quat. Res.*, *57*(1), 91–101.
Mix, A. C., W. Rugh, N. G. Pisias, and S. Veirs (1992), Leg 138 Shipboard sedimentologists, and the leg 138 Scientific Party. Color reflectance spectroscopy: A tool for rapid characterization of deep sea sediments, in *Proc. ODP, Init. Repts.*, vol. 138, edited by L. Mayer, N. Pisias, and T. Janecek, pp. 67–77, Proc. Ocean Drill. Program, College Station, Tex., doi:10.2973/odp.proc.ir.138.104.1992.
Oppo, D. W., J. F. McManus, and J. L. Cullen (1998), Abrupt climate events 500,000 to 340,000 years ago: Evidence from subpolar north Atlantic sediments, *Science*, *279*(5355), 1335–1338.
Ortega-Guerrero, B., M. Caballero-Miranda, S. Lozano-Garcia, and M. de la O Villanueva (1999), Paleoenviromental record of the last 70,000 yr in San Felipe Basin, Sonora desert, Mexico: Preliminary results, *Geofisc. Int.*, *38*, 1–11.
Ortiz, J. D., A. Mix, S. Harris, and S. O'Connell (1999), Diffuse spectral reflectance as a proxy for percent carbonate content in North Atlantic sediments, *Paleoceanography*, *14*(2), 171–186, doi:10.1029/1998PA900021.
Ortiz, J. D., S. B. O'Connell, J. DelViscio, W. Dean, J. D. Carriquiry, T. Marchitto, Y. Zheng, and A. van Geen (2004), Enhanced marine productivity off western North America during warm climate intervals of the past 52 ky, *Geology*, *32*(6), 521–524.
Overpeck, J. T., and J. E. Cole (2006), Abrupt change in Earth's climate system, in *Annual Review of Environment and Resources*, pp. 1–31.
Pahnke, K., and R. Zahn (2005), Southern hemisphere water mass conversion linked with North Atlantic climate variability, *Science*, *307*(5716), 1741–1746.
Paillard, D., L. Labeyrie, and P. Yiou (1996), Macintosh program performs time-series analysis, *Eos Trans. AGU*, *77*, 379, doi:10.1029/96EO00259.
Peltier, W. R. (1994), Ice Age paleotopography, *Science*, *265*, 195–201.
Peterson, L. C., G. H. Haug, K. A. Hughen, and U. Rohl (2000), Rapid changes in the hydrologic cycle of the tropical Atlantic during the last glacial, *Science*, *290*, 1947–1951.

Pichevin, L. E., R. S. Ganeshram, S. Francavilla, E. Arellano-Torres, T. F. Pedersen, and L. Beaufort (2010), Inter-hemispheric leakage of isotopically heavy nitrate in the Eastern Tropical Pacific during the last glacial period, *Paleoceanography*, *25*, PA1204, doi:10.1029/2009PA001754.

Pisias, N. G. (1978), Paleoceanography of the Santa Barbara Basin during the last 8000 years, *Quat. Res.*, *10*, 366–384.

Pisias, N. G., A. C. Mix, and L. Heusser (2001), Millennial scale climate variability of the northeast Pacific Ocean and northwest North America based on radiolaria and pollen, *Quat. Sci. Rev.*, *20*, 1561–1576.

Reyes, A. C., and M. F. Lavin (1997), Effects of the autumn-winter meteorology upon the surface heat loss in the Northern Gulf of California, *Atmosfera*, *10*(2), 101–123.

Roden, G. I. (1962), Oceanographic aspects of the eastern equatorial Pacific, *Geophys. Int.*, *2*, 77–92.

Schmittner, A., and E. D. Galbraith (2008), Glacial greenhouse-gas fluctuations controlled by ocean circulation changes, *Nature*, *456*(7220), 373–376.

Schulz, M., and K. Stattegger (1997), SPECTRUM: Spectral analysis of unevenly spaced paleoclimatic time series, *Comput. Geosci.*, *23*, 929–945.

Siddall, M., T. F. Stocker, R. Spahni, and T. Blunier (2006), Using a maximum simplicity paleoclimate model to simulate millennial variability during the last four glacial cycles, *Quat. Sci. Rev.*, *25*, 3185–3197.

Siddall, M., E. J. Rohling, T. Blunier, and R. Spahni (2010), Patterns of millennial variability over the last 500 ka, *Clim. Past*, *6*(3), 295–303.

Stott, L. D., M. Neumann, and D. Hammond (2000), Intermediate water ventilation on the northeasthern Pacific margin during the late Pleistocene inferred from benthic foraminiferal d13C, *Paleoceanography*, *15*(2), 161–169, doi:10.1029/1999PA000375.

Stott, L., C. Poulsen, S. Lund, and R. Thunell (2002), Super ENSO and global climate oscillations at millennial time scales, *Science*, *297*(5579), 222–226.

Stouffer, R. J., et al. (2006), Investigating the causes of the response of the thermohaline circulation to past and future climate changes, *J. Clim.*, *19*(8), 1365–1387.

Torrence, C., and G. P. Compo (1998), A practical guide to wavelet analysis, *Bull. Am. Meteorol. Soc.*, *79*(1), 61–78.

Turney, C. S. M., A. P. Kershaw, S. C. Clemens, N. Branch, P. T. Moss, and L. K. Fifield (2004), Millennial and orbital variations of El Niño/Southern Oscillation and high-latitude climate in the last glacial period, *Nature*, *428*, 306–310.

van Geen, A., Y. Zheng, J. M. Bernhard, K. G. Cannariato, J. Carriquiry, W. E. Dean, B. W. Eakins, J. D. Ortiz, and J. Pike (2003), On the preservation of laminated sediments along the western margin of North America, *Paleoceanography*, *18*(4), 1098, doi:10.1029/2003PA000911.

van Kreveld, S., M. Sarnthein, H. Erlenkeuser, P. Grootes, S. Jung, M. J. Nadeau, U. Pflaumann, and A. Voelker (2000), Potential links between surging ice sheets, circulation changes, and the Dansgaard-Oeschger cycles in the Irminger Sea, 60–18 kyr, *Paleoceanography*, *15*, 425–442, doi:10.1029/1999PA000464.

van Meerbeeck, C. J., H. Renssen, and D. M. Roche (2009), How did marine isotope stage 3 and Last Glacial Maximum climates differ?—Perspectives from equilibrium simulations, *Clim. Past*, *5*(1), 33–51.

Vellinga, M., and R. A. Wood (2002), Global climatic impacts of a collapse of the Atlantic thermohaline circulation, *Clim. Change*, *54*(3), 251–267.

Wang, X. F., A. S. Auler, R. L. Edwards, H. Cheng, E. Ito, Y. J. Wang, X. G. Kong, and M. Solheid (2007), Millennial-scale precipitation changes in southern Brazil over the past 90,000 years, *Geophys. Res. Lett.*, *34*, L23701, doi:10.1029/2007GL031149.

Wang, Y. J., H. Cheng, R. L. Edwards, Z. S. An, J. Y. Wu, C.-C. Shen, and J. A. Dorale (2001), A high-resolution absolute-dated Late Pleistocene monsoon record from Hulu Cave, China, *Science*, *294*(5550), 2345–2348.

Wang, Y., H. Cheng, R. L. Edwards, X. Kong, X. Shao, S. Chen, J. Wu, X. Jiang, X. Wang, and Z. An (2008a), Millennial- and orbital-scale changes in the East Asian monsoon over the past 224,000 years, *Nature*, *451*(7182), 1090–1093.

Wang, Y., H. Cheng, R. L. Edwards, X. Kong, X. Shao, S. Chen, J. Wu, X. Jiang, X. Wang, and Z. An (2008b), Millennial- and orbital-scale changes in the East Asian monsoon over the past 224,000 years, *Nature*, *451*(7182), 1090–1093.

White, S. M., T. M. Hill, J. P. Kennett, R. J. Behl, and C. Nicholson (2013), Millennial-scale variability to 735 ka: High-resolution climate records from Santa Barbara Basin, Calif., *Paleoceanography*, *28*, 213–226, doi:10.1002/palo.20022.

Wyrtki, K. (1965), The Annual and semi-annual variation of sea surface temperature in the north Pacific Ocean, *Limnol. Oceanogr.*, *10*(3), 307–313.

Yuan, D. X., et al. (2004), Timing, duration, and transitions of the Last Interglacial Asian Monsoon, *Science*, *304*(5670), 575–578.